# Spire-1 contributes to the invadosome and its associated invasive properties.

Vanessa Lagal, Marie Abrivard, Virginie Gonzalez, Audrey Perazzi, Sonam Popli, Elodie Verzeroli, Isabelle Tardieux

© 2014. Published by The Company of Biologists Ltd | Journal of Cell Science (2014) 127, 328–340 doi:10.1242/jcs.130161

RESEARCH ARTICLE

# Spire-1 contributes to the invadosome and its associated invasive properties

**Vanessa Lagal[1,2,3], Marie Abrivard[1,2,3], Virginie Gonzalez[1,2,3], Audrey Perazzi[1,2,3], Sonam Popli[1,2,3], Elodie Verzeroli[1,2,3] and Isabelle Tardieux[1,2,3,*]**

## ABSTRACT

Cancer cells have an increased ability to squeeze through extracellular matrix gaps that they create by promoting proteolysis of its components. Major sites of degradation are specialized microdomains in the plasma membrane collectively named invadosomes where the Arp2/3 complex and formin proteins cooperate to spatiotemporally control actin nucleation and the folding of a dynamic F-actin core. At invadosomes, proper coupling of exo-endocytosis allows polarized delivery of proteases that facilitate degradation of ECM and disruption of the cellular barrier. We investigated the contribution of the actin nucleator Spire-1 to invadosome structure and function, using Src-activated cells and cancer cells. We found that Spire-1 is specifically recruited at invadosomes and is part of a multi-molecular complex containing Src kinase, the formin mDia1 and actin. Spire-1 interacts with the Rab3A GTPase, a key player in the regulation of exocytosis that is present at invadosomes. Finally, over- and under-expression of Spire-1 resulted in cells with an increased or decreased potential for matrix degradation, respectively, therefore suggesting a functional interplay of Spire-1 with both actin nucleation and vesicular trafficking that might impact on cell invasive and metastatic behavior.

**KEY WORDS: Spire-1, Actin, Invadosome, Src-activated 3T3, Gelatin invasion, Endothelial transmigration, Vesicular trafficking**

## INTRODUCTION

Whereas cells from myeloid and lymphoid lineages are typically endowed with the physiological capability to glide through the extracellular matrix (ECM) network and to cross endothelia to fulfil their functions, tumor cells in general have gained similar abilities as they squeeze through ECM gaps and endothelia and eventually infiltrate tissues. Whether constitutive or adaptive, these processes are often, although not always, associated with local proteolysis of the surrounding matrix (Sabeh et al., 2009; Linder et al., 2011; Wolf and Friedl, 2011). Major sites of matrix degradation are specialized mechano-sensitive membrane microdomains that adhere to the substratum: these are either called invadopodia or podosomes depending whether they form in cancer cells or in myeloid-derived and *v-Src*-transformed cells, respectively and are collectively termed invadosomes (Linder, 2007; Parekh and Weaver, 2009; Weaver, 2008). Indeed, expression of the constitutively active *Src* oncogene induces transcription of genes whose products have been implicated in tumor cell growth and metastatic properties (Irby and Yeatman, 2000). Chief among these products is the Src family kinase itself, which drives the remodeling of the actin cytoskeleton from stress fibers to podosomes (Tarone et al., 1985; Destaing et al., 2010; Cougoule et al., 2010; Boateng et al., 2012).

Actin nucleation plays a central role in promoting the multipartite architecture of all types of invadosomes. A core of dynamic F-actin bundles folds under the tight control of actin-nucleating and -elongation factors and actin-related signaling proteins (Albiges-Rizo et al., 2009; Dovas et al., 2009; Sibony-Benyamini and Gil-Henn, 2012). Within this core, synergistic activation of N-WASP and cortactin promotes continuous stimulation of the Arp2/3 complex to nucleate branched actin daughter filaments. Recently, a second class of actin nucleators composed of the DRF/mDia1-3 (human/mouse) formins have been shown to cooperate with the Arp2/3 complex during invadosome biogenesis and to selectively localize at invadosomes in primary macrophages (Lizárraga et al., 2009; Mersich et al., 2010). Finally, invadosomes can self-organize into dynamic clusters or rosettes by building up a network of radial actin filaments that connects individual structures to each other (Albiges-Rizo et al., 2009; Destaing et al., 2010; Linder et al., 2011).

The proteolytic and pro-invasive properties of invadosomes are supported by intense polarized vesicular traffic with the endocytic and exocytic pathways locally converging and promoting delivery of ECM lytic enzymes. The large family of soluble and membrane-associated zinc-dependent metalloproteases (MT-MMPs), together with additional proteolytic enzymes, direct a diffuse and/or cell-surface-restricted lysis of the ECM (Egeblad and Werb, 2002; Caldieri and Buccione, 2010; Linder et al., 2011). Consequently, the membrane fusion machinery that regulates exocytosis is functionally required for ECM degradation and invasion (Steffen et al., 2008). However, there is increasing evidence that actin nucleation ensures correct membrane trafficking along the endocytic or exocytic pathways (Kaksonen et al., 2006; Soldati and Schliwa, 2006; Morel et al., 2009) and the Arp2/3 regulatory partner N-WASP has been shown to promote delivery and stabilization of MTP1-MMP at invasive pseudopodia in 3D matrices (Yu et al., 2012).

Spire proteins not only belong to a class of actin nucleators (Quinlan et al., 2005; Renault et al., 2008; Firat-Karalar and Welch, 2011) but have also been assigned a role in vesicular trafficking, in particular from the TGN to the plasma membrane (Quinlan et al., 2005; Kerkhoff et al., 2001). More recently, a fascinating study has revealed that Spire protein in concert with formin can organize a newly identified network that connects cytoplasmic vesicles to each other and drives their long range and

[1]INSERM, U1016, Institut Cochin, 22 Rue Méchain, 75014 Paris, France. [2]CNRS, UMR8104, 22 Rue Méchain, 75014 Paris, France. [3]Université Paris Descartes, Sorbonne Paris Cité, 22 Rue Méchain, 75014 Paris, France.

*Author for correspondence (email: isabelle.tardieux@inserm.fr)

**Received 28 February 2013; Accepted 15 October 2013**



Journal of Cell Science

Journal of Cell Science (2014) 127, 328–340 doi:10.1242/jcs.130161

polarized transport to the plasma membrane (Schuh, 2011). Therefore, we investigated whether, in mammalian cells, Spire could contribute to invadosome structure and function. Spire proteins, including human Spire-1 and Spire-2, all display a conserved modular structure with a N-terminally located kinase non catalytic C-lobe domain (KIND) followed by a central cluster of four G-actin binding Wiskott–Aldrich syndrome protein homology domain 2 (WH2) modules powering the actin-nucleating activity. The C-terminal region contains: (1) a 'Spire-box' with sequence similarity to a helical domain of rabphilin-3A; and (2) a zinc finger structure that is highly homologous to the membrane-binding FYVE motif; both motifs are reported to be responsible for targeting of Spire-1 to intracellular membranes (Kerkhoff et al., 2001; Kerkhoff, 2006).

We found a significant upregulation of Spire-1 expression in Src-activated fibroblasts and pre-osteoclasts, two prototypes of invadosome-forming cells. Both endogenous and exogenous Spire-1 accumulated at invadosomes and at rosettes or rings, a localization that fits with the detection of Spire-1 within a multi-molecular complex also containing bona fide invadosome components such as the phosphorylated Src kinase (pY418-Src), the formin mDia1 and F-actin. Spire-1 also localized to cytoplasmic vesicles whose traffic towards invadosomes might involve the GTPase Rab3A because we show a partnership between the two molecules in cells and *in vitro*. Because modulation of Spire-1 expression impacts cell proteolytic and pro-invasive properties, our data support a tight interplay between three types of actin nucleators during fine-tuning of invadosome function and newly highlight Spire-1 as one player that possibly couples actin nucleation and vesicular trafficking during invadosome function.

## RESULTS

### Spire-1 expression is enhanced in Src-transformed cells and is detected at invadosomes or rings

Because expression of Spire-1 is reported to be tissue-restricted, with a prominence in embryonic and adult brain cells, we first verified whether Spire-1 was expressed in cells characterized by their high number of invadosomes. Following RNA extraction, RT-PCR assays were carried out using pairs of primers that discriminate between *Spire1* and *Spire2* sequences (see Materials and Methods). A single 1123 bp PCR product was detected in parental and Src-activated (3T3-Src$^+$) mouse 3T3 fibroblasts or in Src-activated mouse pre-osteoclasts (pre-Ost-Src$^+$) that was barely distinguishable in 3T3 mouse parental fibroblasts (3T3-WT; Fig. 1A). The identity of the PCR product as *Spire1* was confirmed by nucleotide sequencing (data not shown). We found that the amount of these transcripts is significantly enhanced in Src$^+$ when compared with wild-type (WT) cells (about six- to eightfold, Fig. 1A). To quantify and localize Spire-1 protein *in situ* in Src$^+$ cells, we first checked for the specificity of commercial antibodies raised against the Spire-1 internal region (K19). Using SDS-PAGE and western blotting, we analyzed whole-cell extracts from HEK-293 cells expressing endogenous Spire-1, and we detected a single product at the expected size, for which signal intensity correlated with the amounts of extracts (black labels, Fig. 1B). When HEK-293 cells ectopically expressed Myc-Spire-1 fusion protein (red labels, Fig. 1B), the K19 antibodies recognized several products equally detected by anti-Myc antibodies. Antibody specificity was further confirmed with the loss of signal in cells silenced for Spire-1 (supplementary materia Fig. S1). We next analyzed cell extracts from the different cell lines of interest at two protein concentrations and we observed a ~threefold increase in Src$^+$ cells when compared with 3T3-WT cells (Fig. 1C). However, because these antibodies appeared ineffective for *in situ* analysis, we generated antibodies raised against the recombinant Spire-1 N-KIND-terminal polypeptide (N-KIND; supplementary material Table S1). As expected, these antibodies detected endogenous Spire-1 and exogenous Myc-Spire-1 in HEK293 total cell extracts (Fig. 1B, right). When used *in situ* on 3T3-Src$^+$cells, these antibodies labeled ring-shaped structures at the cell periphery that resembled invadosomes and rosettes (Fig. 1D, white arrows). Co-staining of F-actin that typically accumulates in those structures supported the presence of Spire-1 at individual (arrowheads) and clustered (arrows) invadosomes (Fig. 1E).

### Spire-1 is selectively recruited to invadosomes and is part of a multi-molecular complex containing mDia1, actin and the pY418-Src kinase

We next analyzed the distribution of endogenous Spire-1 in more detail with regards to additional bona fide invadosome components. Because Spire-1 fusion proteins proved useful for unravelling how Spire-1 participates in endosome biogenesis (Morel et al., 2009) and since endogenous and Myc-tagged Spire-1 signals overlapped in 3T3-Src$^+$ cells (supplementary material Fig. S2A, green and red arrows), we included samples of cells expressing GFP or Myc-tagged Spire-1 in the study.

In 3T3-Src$^+$ cells, whereas endogenous Spire-1 displayed a punctate cytoplasmic pattern in line with previous work reporting the distribution of exogenous p150-Spire protein (Kerkhoff et al., 2001), it also markedly associated with peripherally located invadosomes that were unambiguously identified by the co-labeling of cortactin and F-actin (Artym et al., 2006) (Fig. 2A; supplementary material Fig. S2B). A similar overlap was observed between Myc-Spire-1 (arrows), Cortactin and F-actin in transfected 3T3-Src$^+$ cells [Fig. 2B,C, see insets and Pearson's colocalization coefficients (Bolte and Cordelières, 2006)] and was also found with the GFP-Spire-1 fusion protein (supplementary material Fig. S2C). Another key component of the invadosomes, the pY418-Src kinase was seen decorating the edges of Myc-Spire-1-labeled invadosomes and rosettes (see arrows and the zoomed area, Fig. 2D). Finally, using affinity pull-down assays to co-precipitate Myc-Spire-1 with binding partners from 3T3-Src$^+$ cells, we found Myc-Spire-1 in a complex containing not only actin and pY418-Src but also the formin mDia1 ($n>4$ independent experiments) (Fig. 2E). Interestingly, neither Arp2/3 nor cortactin was detected within the Spire-1 multi-molecular complex under our conditions. Because mDia1 and endogenous Spire-1 were observed as distinct populations in the 3T3-Src$^+$ cell cytoplasm in contrast to invadosomes or ring sites (Fig. 2F; supplementary material Fig. S2E, see also higher-magnification insets and Pearson's coefficient), our data suggest a novel interplay between Spire-1 and mDia1 that is independent of the Arp2/3 actin-nucleating complex – specifically at invadosome sites. This observation agrees well with previous and recent reports of the cooperation of Spire-1 and formin during asymmetric division of *Drosophila* and mouse oocytes (Quinlan et al., 2007; Vizcarra et al., 2011; Pfender et al., 2011).

### The Spire-1 WH2 domain targets Spire-1 to invadosomes

Because *in situ* and biochemical data pointed to Spire-1 as an actin partner protein at invadosomes, we next tested whether the four WH2 modules that confer the actin-nucleating property would control targeting of Spire-1 to invadosomes. To this end, we analyzed the subcellular distribution of transiently expressed truncated Spire-1 proteins with or without the WH2 domain in

Journal of Cell Science (2014) 127, 328–340 doi:10.1242/jcs.130161

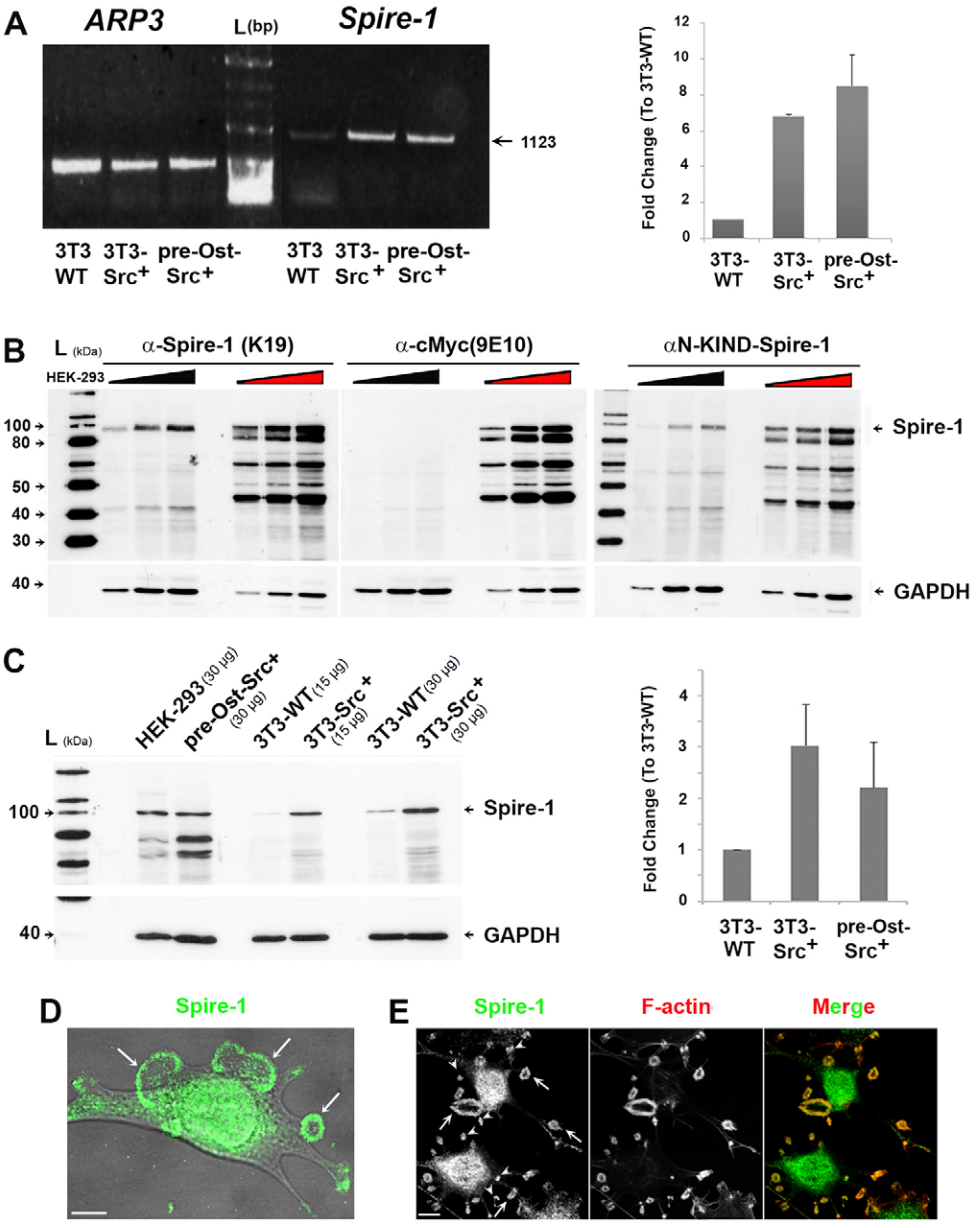


**Fig. 1. Spire-1 expression is enhanced in Src$^+$ cells and is detected at the cell periphery in actin-enriched invadosome-like structures.** (A) *Spire1* transcripts were detected in total RNA and quantified (histogram data are from four independent experiments using two different batches of RNA). The *Arp3* gene was used as reference; L, ladder (bp). (B) Specificity of the anti-Spire-1 K19 (Santa Cruz) and the N-KIND-Spire-1 antibodies was controlled on whole-cell extracts from $5\times10^4$ to $5\times10^5$ HEK-293 cells (black labels) and from HEK-293 cells expressing a Myc-Spire-1 fusion protein (red labels). The reliability of the detection was assessed with an anti-Myc antibody (9E10) whereas the GAPDH protein served as loading control. L, ladder (kDa) (C) Spire-1 protein expression was quantified on 15 and 30 µg of 3T3-WT and 3T3-Src$^+$ cell lysates and 30 µg of pre-osteoblast-Src$^+$ using anti-Spire-1 K19 antibodies. 30 µg of HEK-293 cell extract served as control and GAPDH protein as reference (histograms are derived from five independent assays). L: ladder (kDa). (D,E) *In situ* localization of Spire-1 in 3T3-Src$^+$ cells using N-KIND-Spire-1 antibodies (green) and (E) co-stained with Phalloidin to detect F-actin (red). White arrows show invadosomes and rosettes (D); arrowheads and arrows indicate individual and clustered invadosomes, respectively (E). Scale bars: 10 µm.

Src$^+$ fibroblasts (see schematic representation of the constructs supplementary material Fig. S3A). Invadosomes were detected using Phalloidin staining of their F-actin cores as exemplified with full-length Myc-Spire-1 (Fig. 3A). When the N-terminal KIND (N-KIND) domain was expressed alone, it was distributed in a more diffuse cytoplasmic pattern than full-length Spire-1 and only ~22% of cells showed a modest enrichment of the Myc-N-KIND polypeptide at invadosomes ($n$=300 cells) (Fig. 3B, supplementary material Fig. S3B). By contrast, the N-KIND WH2 domain was systematically enriched at invadosomes ($n$=250 cells, Fig. 3C, supplementary material Fig. S3C). Whereas the Myc-C-terminal Spire-1 (Myc-Cter) polypeptide displayed a vesicular pattern similar to Spire-1 and it localized at invadosome sites in less than 5% of the cells ($n$=250 cells) (Fig. 3D). However, the addition of the WH2 domain promoted a striking accumulation of the polypeptide at all invadosomes for all the cells screened ($n$=250, Fig. 3E, supplementary material Fig. S3D). Of note, similar results were obtained when the Myc tag was replaced by an HA tag fused to the C-terminal (Cter) polypeptide (less than 3% HA-positive invadosomes, $n$=200, supplementary material Fig. S3E). These data indicate that the WH2 domain drives Spire-1 at invadosomes. Interestingly, a highly significant increase in the number of invadosomes and rosettes was only associated with cells expressing Myc-WH2 when compared with cells expressing Myc-Spire-1 or mock-transfected cells (Ct) (Fig. 3F, see arrows; Fig. 3G, Student's $t$-test, $P<0.01$). Surprisingly, when the recombinant polypeptides encompassed the WH2 domain with either the N- or C-terminal regions (Fig. 3G) the number of invadosomes and rosettes did not significantly differ from that in cells expressing Myc-Spire-1 ($n$=3 independent assays, each in triplicate). We thus hypothesized that the adjacent domains could modulate the properties of the WH2 domain. When extracts of HEK-293 cells expressing Myc-Spire-1, Myc-N-KIND or HA-Cter were incubated with immobilized recombinant GST-WH2 (Fig. 4A, left) or GST polypeptides (Fig. 4B), Spire-1 and the Cter but not

Journal of Cell Science (2014) 127, 328–340 doi:10.1242/jcs.130161

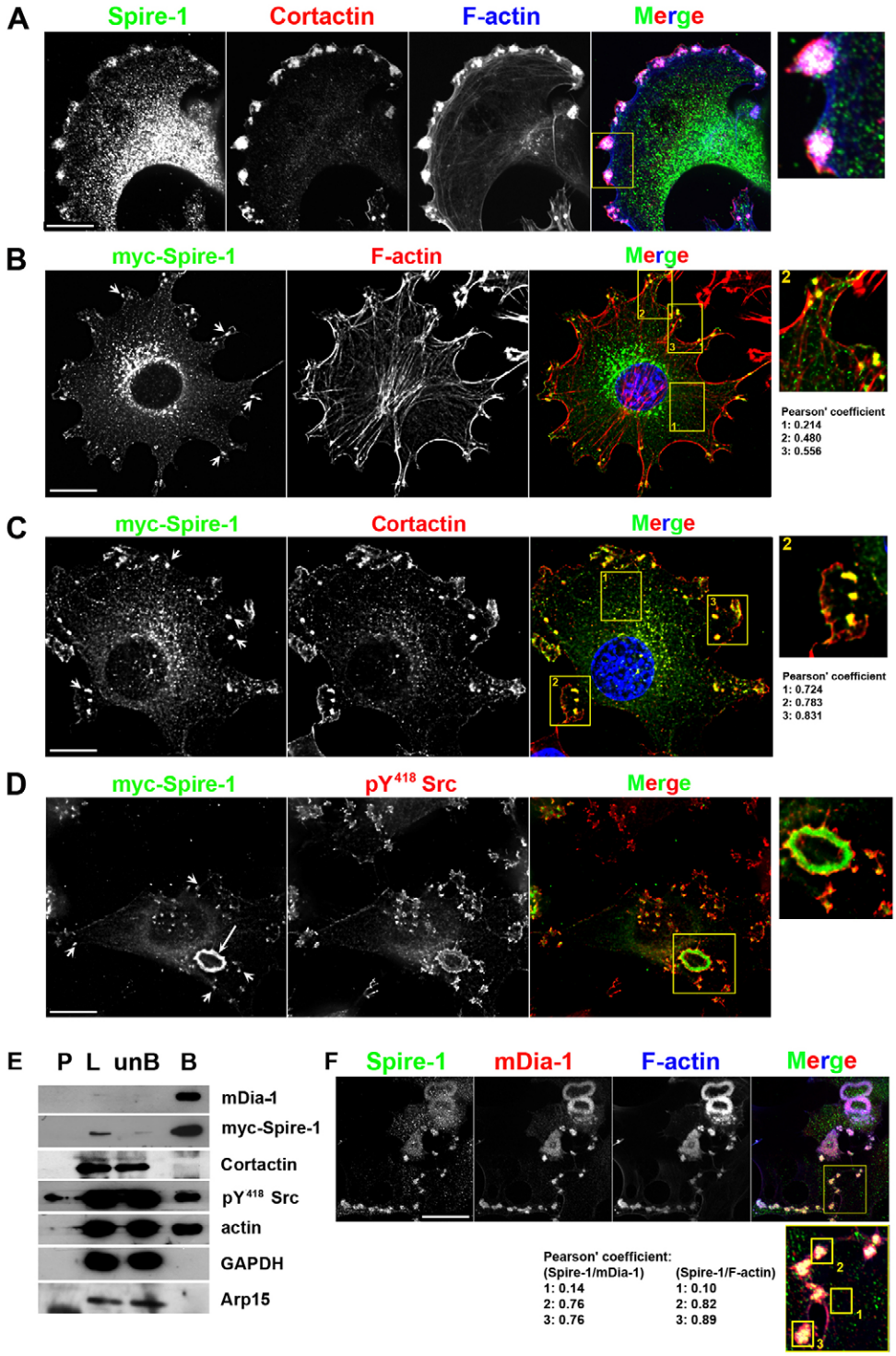


**Fig. 2. Myc-Spire-1 is selectively recruited to invadosomes and is part of a multi-molecular complex containing mDia1, actin and Src kinase.** (A) Triple immunofluorescent labeling of 3T3-Src$^{+}$ cells using N-KIND-Spire-1 (green), anti-cortactin (red) antibodies and Phalloidin (F-actin, blue). F-actin- and cortactin-enriched invadosomes are also enriched with Spire-1, see zoom inset (right). (B–D) Double immunofluorescent labeling of 3T3-Src$^{+}$ cells expressing Myc-Spire-1 using anti-Myc c9E10 antibodies (green) and either anti-cortactin, anti-pY418-Src or phalloidin (red). Nuclei were additionally stained with DAPI (blue) (B,C). Note the short and long arrows marking individual and clustered invadosomes, respectively. Framed areas shown in the merge images are zoomed in right panels and Pearson's colocalization coefficients are indicated below. (E) Myc-Spire-1 was immunoprecipitated from 3T3-Src$^{+}$ cells using anti-Myc antibodies. Whereas formin (mDia1), pY418-Src and actin co-eluted with Myc-Spire-1, neither the Arp2/3 complex nor its regulatory component cortactin were found within the complex. GAPDH served as a negative control. P, pellet; L, lysate; unB, unbound; B, bound. (F) 3T3-Src$^{+}$ cells were co-stained with N-KIND-Spire-1 (green) and anti-mDia1 antibodies (red) and with Phalloidin (blue). Framed area shown in the merge image is zoomed in the bottom panel and Pearson's coefficients quantify signal colocalization. Scale bars: 10 μm.

the N-KIND domain selectively and systematically co-eluted with the GST-WH2 ($n$=9 independent assays), whereas no co-elution was detected with GST alone ($n$=3 independent assays). The specificity of the interaction was validated using extracts from cells expressing large amounts of the highly soluble HA-cofilin fusion protein in the co-purification assay because we never detected the protein in the GST-WH2 eluates ($n$=3 independent assays) (Fig. 4A, right). Of note, when the membranes were probed to detect actin, we found that actin was efficiently captured by the WH2 polypeptides, including when the latter interacted with the HA-Cter domain. Thus, under these conditions, the intra-domain interaction is unlikely to interfere with the actin binding properties. Finally, in *in vitro* assays using recombinant polypeptides purified from *E. coli* cells, GST-WH2 polypeptides were retained by His-GST-Cter (Fig. 4C, black arrows) but not by His-GST-N-KIND that was immobilized on nickel beads (Fig. 4C). Collectively, these data suggest that Spire-1 can either adopt a conformation induced by intramolecular interaction between the central WH2 and the C-terminal domains of the protein or instead that Spire-1 homo-dimerizes for optimal function.

Journal of Cell Science (2014) 127, 328–340 doi:10.1242/jcs.130161

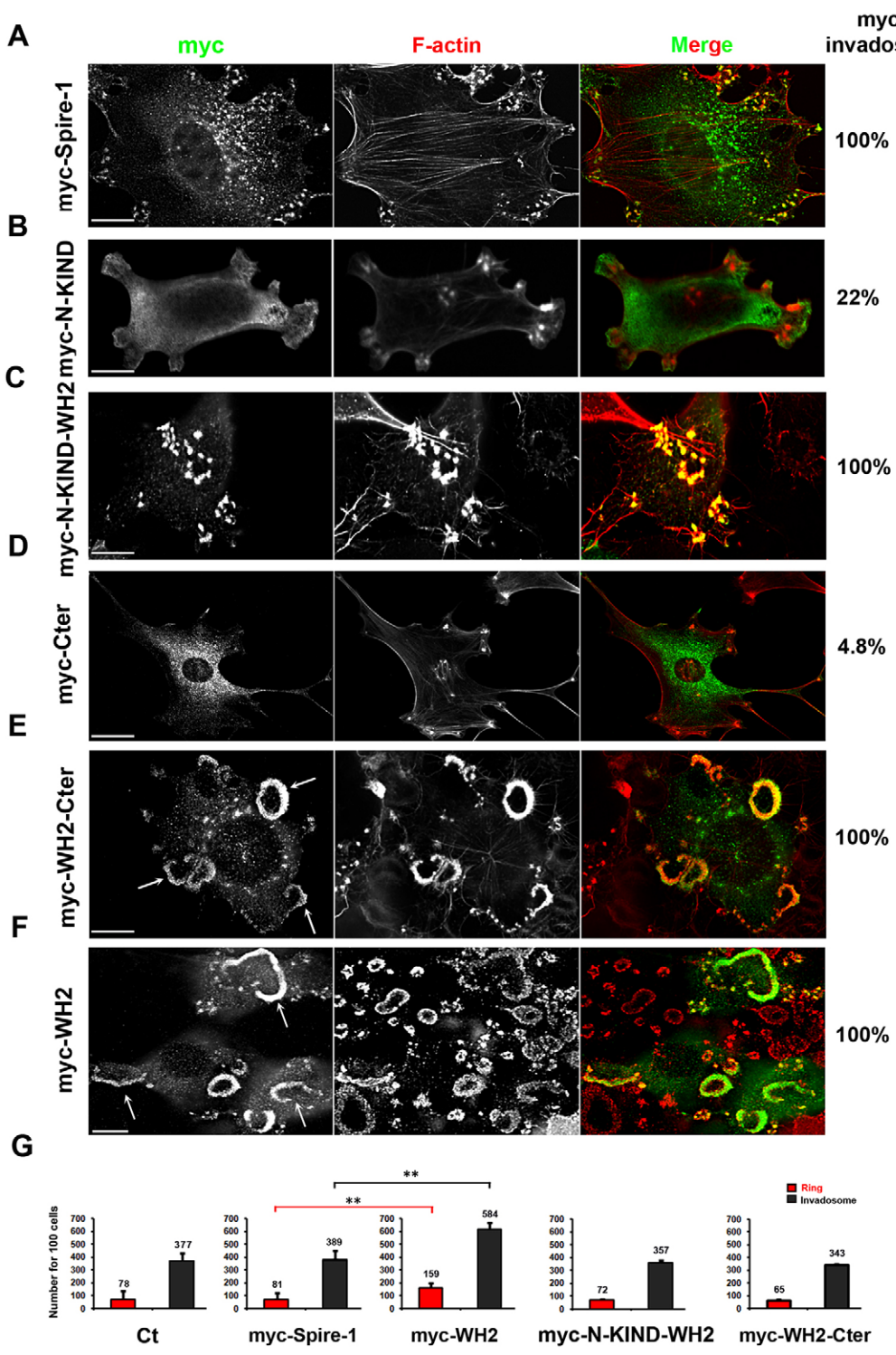


**Fig. 3. The Spire-1 WH2 domain drives Spire-1 to invadosomes.** 3T3-Src$^{+}$ cells expressing Myc-Spire-1 (A) or truncated Spire-1 fusion proteins (B–F) were labeled with anti-Myc antibodies (green) and with phalloidin to detect F-actin (red). Note the large rosettes indicated by white arrows (E,F). Percentage of cells for which F-actin-labeled invadosomes are positive for Myc-tagged Spire-1 polypeptides of interest are shown on the right ($200<n>300$ cells). Scale bars: 10 μm. (G) Histograms show the number of rings or rosettes (red), or individual invadosomes (gray) for 100 cells; average numbers from triplicates are indicated. Statistical analysis was performed using the Student's *t*-test; $^{*}P<0.05$. Note that the presence of WH2 domain was required for Spire-1 localization at invadosomes and that addition of the N- or C-terminal domains regulated the enhanced effect of WH2 domain on invadosome and ring numbers.

### Rab3A interacts with the Spire-1 C-terminal region

Regulated exocytosis is a prominent feature of invadosome activity and RabGTPases are the major regulators of polarized trafficking of vesicles to recipient membranes. Interestingly, the homology of the Spire box and the rabphilin-3A α-helix suggests a contribution of this domain in the association of Spire with a small RabGTPase. Within the large RabGTPase family, many are involved in cancer progression, both as inhibitory and promoting factors (Ho et al., 2012). Although Rab3A plays a major role in regulating exocytosis in a number of neuronal and endocrine cells (Baldini et al., 1995; Leenders et al., 2001; Pavlos et al., 2010), as well as in sperm (Bustos et al., 2012), it also has a role in cancer cells: *Rab3A* is upregulated in insulinoma but not in normal islets of pancreatic tissue (Lankat-Buttgereit et al., 1994). Rab3A protein is overexpressed in aggressive breast stem-like tumor cells and in epithelial breast cancer cells in response to Heregulin (Vadlamudi et al., 2000) as well as in myofibroblasts (Ina et al., 2005). Interestingly, we found a modest increase in Rab3A protein

Journal of Cell Science (2014) 127, 328–340 doi:10.1242/jcs.130161

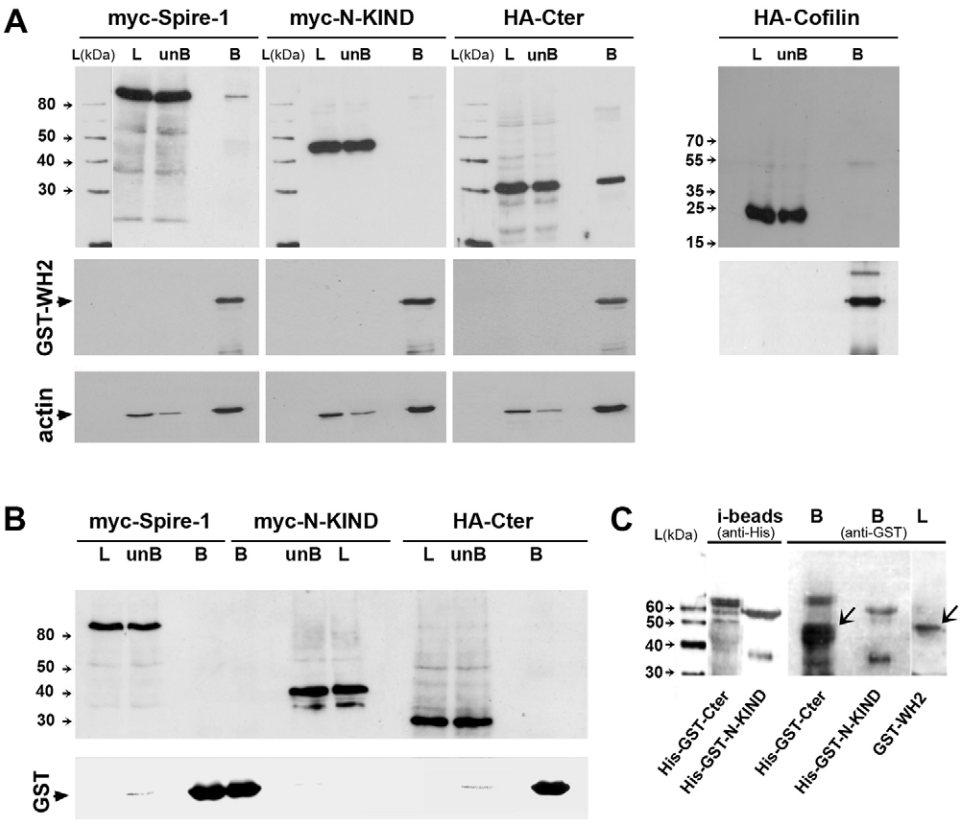


**Fig. 4. The Myc-Spire-1 C-terminal domain binds to the WH2 domain.** (A) Western blot showing that cell extracts containing Myc-Spire-1 and HA-Cter but not Myc-N-KIND were captured by immobilized GST-WH2 polypeptides. The specificity of the capture was controlled by (1) using HA-cofilin-containing cell extracts (right panel) and (2) conducting the same assays on immobilized GST (B). Actin was detected in all the GST-WH2 eluates suggesting that the interaction between the Spire-1 domains does not regulate the actin-binding properties to actin of the WH2 motifs (A, bottom panel). (C) Bacterially expressed His-GST-Cter and N-KIND domains were purified and immobilized on nickel beads (i-beads) as assessed with anti-His antibodies and further capture of the GST-WH2 domain was assessed using anti-GST antibodies. P, pellet; L, lysate; unB, unbound; B, bound.

expression of about 1.6- and 2.8-fold in Src$^+$ when compared with 3T3-WT cells (supplementary material Fig. S4A). Moreover, a pool of endogenous Rab3A accumulated at invadosomes and rosettes in dot-like vesicles in 3T3-Src$^+$ cells (Fig. 5A; supplementary material Fig. S4B, see the higher magnification of insets 1 and 2 in right panels). When these cells co-expressed Myc-Spire-1 and GFP-Rab proteins, a significant overlap was seen between Myc-Spire-1 and GFP-Rab3A (Fig. 5B and Pearson's coefficients) but not between Myc-Spire-1 and the early endosomal marker GFP-Rab5A (Fig. 5C). The coincident Rab3A and Myc-Spire-1 signals marked individual and clustered invadosomes (Fig. 5B). Because a Spire-1 and Rab3A GTPase interaction has not yet been reported, we next checked whether both proteins could co-purify under pull-down assay conditions. When Myc-Spire-1 was immunoprecipitated from Src$^+$ cells expressing Myc-Spire-1 with either GFP-Rab3A or GFP-Rab5A, only GFP-Rab3A was pulled down as a Spire-1 partner (Fig. 5D, $n=5$ independent experiments). This binding was confirmed *in vitro* using immobilized recombinant GST-Rab3A and extracts from HEK-293 cells expressing several truncated Spire-1 constructs (Fig. 5E): Myc-Spire-1 indeed bound to GST-Rab3A as did the Cter domain, in contrast to the N-KIND domain, whereas none of the recombinant proteins or polypeptides co-eluted with GST alone (data not shown). Since p150-Spire-1 was reported to colocalize with Rab11 and to function along the exocytic pathway (Kerkhoff et al., 2001; Schuh, 2011) and since a subset of GTPases including Rab8A were recently implicated in the release of MTP1-MMP at the plasma membrane in primary macrophages (Wiesner et al., 2013), we checked whether any of these could be recruited at invadosomes. By analysing the distribution of GFP-Rab7A, GFP-Rab8A or GFP-Rab11A expressed in 3T3-Src$^+$ cells, we often observed GFP-Rab7A and GFP-Rab11A in the vicinity of invadosomes as vesicles, but only GFP-Rab8A was detected partially overlapping with F-actin-marked invadosomes (supplementary material Fig. S5C, see also the magnified area as insets at the bottom). When cells co-expressed GFP-Rab8A and Myc-Spire-1, many coincident dot-like signals were observed (supplementary material Fig. S6A, white arrow), including at the edges of invadosomes and rosettes well labeled with Phalloidin (supplementary material Fig. S6A, white arrowheads) possibly suggesting a wider interplay between Rab proteins and Spire-1. Of note, overexpression of Rab7A was also accompanied by a significant reduction in the number of invadosomes (data not shown). Collectively, our data support a specific partnership between Spire-1 and Rab3A that contributes to invadosomes and might function in concert with other Rab proteins, notably Rab8A.

### The level of Spire-1 expression modulates degradation of the extracellular matrix

The results suggesting a partnership between Spire-1 and Rab3A prompted us to verify whether Spire-1 could modulate invadosome-mediated functions. Although we could not obtain a reliable downregulation of Spire-1 in 3T3-Src$^+$ cells despite using several siRNA sequences, we succeeded in decreasing the level of expression to 45% of that in control cells when using human breast cancer MDA-MB-231 cells. This is a common cell line model used to study invadosome-mediated matrix degradation, in particular when MMPs are overexpressed (Artym et al., 2006) (Fig. 6A). Therefore we assayed whether decreasing Spire-1 expression could impair the ability of MDA-MB-231 cells to degrade matrix by interfering with proper delivery of proteases at invadosomes. To this end, cells were silenced for Spire-1 expression (*si*Spire-1) while transfected to express the fusion MT1-MMPmCherry protein (see Materials and Methods). As a positive control, we also silenced expression of

Journal of Cell Science (2014) 127, 328–340 doi:10.1242/jcs.130161

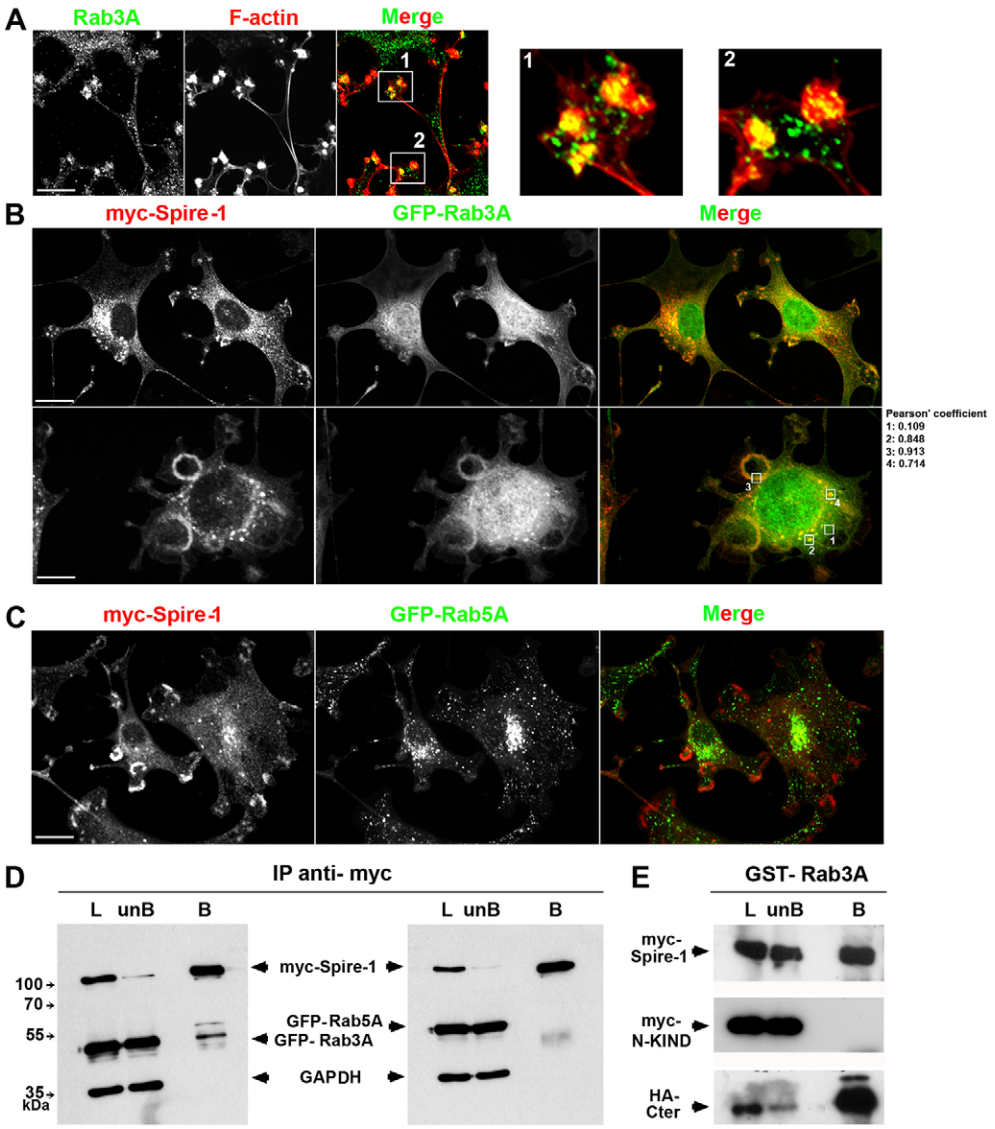


**Fig. 5. Rab3A colocalizes with Spire-1-positive invadosomes and interacts with the C-terminal but not the N-terminal domain of Spire-1.** (A) Double immunofluorescent labeling of 3T3-Src$^{+}$ cells with anti-Rab3A antibodies (green) and Phalloidin (F-actin, red). Framed areas 1 and 2 shown in the merge image are zoomed in right panels 1 and 2. Note that Rab3A-positive vesicles converge at the F-actin core of invadosomes. 3T3-Src$^{+}$ cells co-expressing Myc-Spire-1 and GFP-Rab3A (B) or GFP-Rab5A (C) were stained with anti-Myc antibodies (red). Framed areas in the merge image are used to quantify colocalization (B) using Pearson's coefficient. Scale bars: 10 μm. (D) Myc-Spire-1 was immunoprecipitated from 3T3-Src$^{+}$ cells co-transfected with Myc-Spire-1 and either GFP-Rab3A or GFP-Rab5A. Rab3A (left) but not Rab5A (right) co-eluted with Myc-Spire-1. GAPDH served as internal control protein loading. Molecular mass is indicated in kDa. (E) Recombinant GST-RAb3A was immobilized on beads and incubated with HEK-293 cell extracts expressing Myc-Spire-1, Myc-N-KIND or HA-Cter domains. Western blot shows that full-length Spire-1 and the HA-Cter but not the N-KIND-domain interact with Rab3A. L, lysate; unB, unbound; B, bound.

cortactin (siCort, 89% of signal extinction) since it was reported to impair MDA-MB-231 matrix proteolytic activity (Artym et al., 2006) (supplementary material Fig. S5B). Gelatin degradation was subsequently measured after 6 hours of contact with cells by quantifying the loss of fluorescent signal associated with cells. When compared with cells transfected with irrelevant siRNA oligonucleotides (Ct), MT1-MMP-mCherry-expressing cells silenced for cortactin or for Spire-1 exhibited a decrease of about 60% and 36% in their capacity to degrade gelatin, respectively (Fig. 6C,D). Conversely, we tested whether increasing the level of Spire-1 expression could enhance invadosome proteolytic function in 3T3-Src$^{+}$ cells. The gelatin-degradation assay was kept identical except the cells were transfected to express Myc-Spire-1. Although F-actin and Myc-Spire-1 incorporated at invadosomes and at some cell protrusions, these domains topologically correlated with area of digested gelatin (Fig. 7A, white arrows). Sampling cells that either weakly or strongly overexpressed Myc-Spire-1 by measuring pixel intensity per cell area (high and low, respectively, Fig. 7B,C) highlighted a significant correlation between the level of Myc-Spire-1 expression and cell proteolytic activity ($n$>60 cells). The number of cells associated with substrate digestion was only increased significantly in 3T3-Src$^{+}$ cells expressing high level of Myc-Spire-1 when compared with low or undetectable levels of Spire-1 expression in the same field of observation (Fig. 7B,C,F,G). As additional controls, 3T3-Src$^{+}$ cells expressing Myc-Spire-1 that were exposed to the potent broad spectrum metalloprotease inhibitor batimastat (BB94, 10 μM) during the assay were unable to degrade the matrix (Fig. 7D,G) although they exhibited an intact actin cytoskeleton and invadosomes. By contrast, overexpression of MT1-MMP-mCherry strongly promoted matrix degradation activity (Fig. 7E,G). Collectively, our functional assays suggest that Spire-1 is involved in promoting metalloprotease-dependent proteolytic activity on the matrix at active invadosomes.

### Overexpression of Myc-Spire-1 associates with an increase in cell-invasion properties

Leukocytes and cancer cells elicit physiological and dysregulated properties that support their ability to invade not only the ECM but also cellular monolayers, in particular at the vasculature level. Because endothelial cells line the blood vessel walls, we next investigated whether Spire-1 expression could correlate with cell invasiveness. To this end, we took advantage of the human brain endothelial capillary cell line (hCMEC/D3) that organizes as a

Journal of Cell Science (2014) 127, 328–340 doi:10.1242/jcs.130161

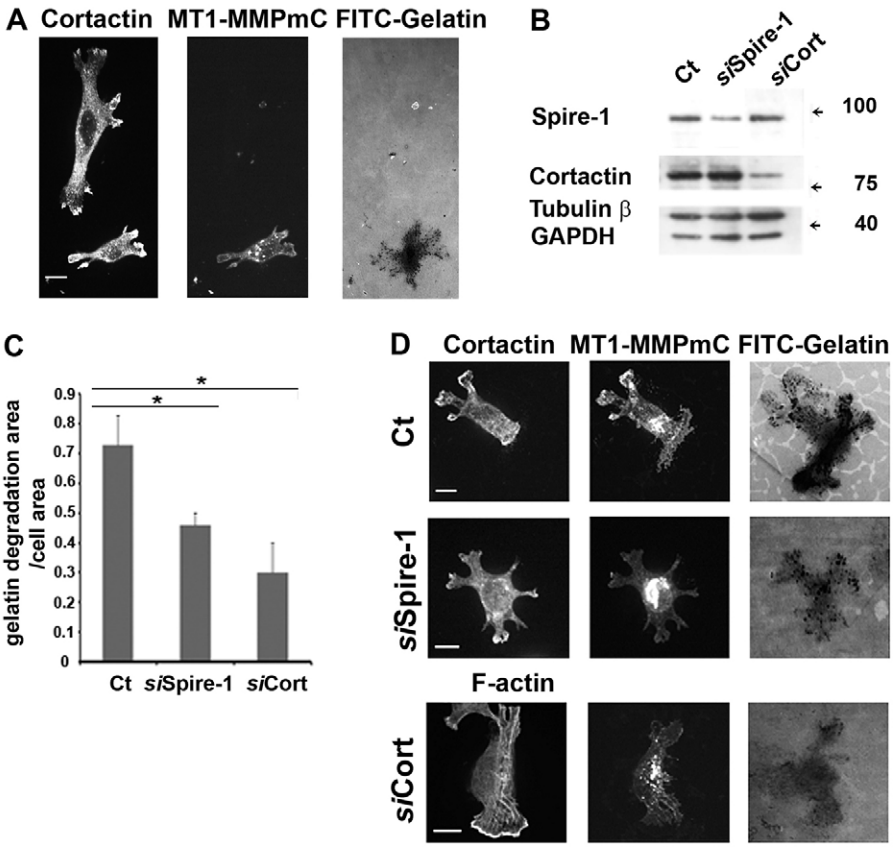


**Fig. 6. Silencing of human Spire-1 in MDA-MB-231 cells reduces gelatin matrix degradation.** (A) MT1-MMP-mCherry (MT1-MMP-mC) overexpressing MDA-MB-231 cells were associated with a much more pronounced gelatin-degradation area when compared with cells that did not express MTP1-MMP-mC. Cells were stained with anti-cortactin antibodies (B) Western blots show the levels of silencing of Spire-1 (*si*Spire-1) and Cortactin (*si*Cort) for $10^5$ MDA-MB-231 cells expressing MT1-MMP-mC. Cells (Ct) treated with AllStars Negative Control siRNA (Qiagen) were used as controls whereas tubulin-β and GAPDH were used as internal loading controls. Molecular mass is shown in kDa. (C,D) $10^5$ cells of the silenced cell populations were cultured on a FITC-gelatin layer for 6 hours. Areas of cells and fluorescence loss in MT1-MMPmC-expressing cells were quantified using ImageJ software. (C) Histograms represent the ratio of area of gelatin degradation to the cell area for control (Ct), Spire-1 (*si*Spire-1)- and cortactin (*si*Cort)-silenced cells (two independent experiments, for each $n=40$ cells expressing the MT1-MMP-mC protein). Statistical analysis was performed using the Student's *t*-test, $^*P<0.05$. (D) Ct and Spire-1-silenced cells were stained with anti-cortactin antibodies and cortactin-silenced cells were labeled with Phalloidin. Areas of gelatin matrix degradation appeared as dark spots: note the decrease of digested gelatin area for Spire-1- and cortactin-silenced cells when compared with Ct cells. Scale bars: 10 μm.

functional endothelial barrier (Weksler et al., 2005). We used the impedance-based *xCELLigence* RTCA device that allows real-time measurement of the changes in electrical resistance of a cell monolayer adhering on top of gold electrodes placed at the bottom surface of microplates. Impedance values are further translated into cell indexes (CI) that increase with culturing time to reach a characteristic plateau for each barrier-forming cell type. A CI of about 7 corresponds to a tight functional cellular barrier routinely obtained with hCMEC/D3 after 40 hours of culture under our conditions. Barrier integrity was assessed by adding hyper-osmolar mannitol that instantaneously destabilizes the tight junctions between adjacent cells (Luissint et al., 2012) and induced a rapid and substained drop in CI (Fig. 8A, top graph). When single-cell suspensions were added to the endothelial layer, CIs dropped according to the extent of disturbance and the duration of barrier integrity. 3T3-WT fibroblasts (pink line) that do not form invadosomes and do not efficiently invade monolayers had a moderate effect on the endothelium cell index, in contrast to invasive 3T3-Src$^+$ cells (dark green line) (Fig. 8A, bottom panel). Of note, drops in the CI were more pronounced for 3T3-Src$^+$ cells overexpressing either Myc-WH2 (light blue) or Myc-Spire-1 (dark blue) when compared with cells expressing a Myc-irrelevant polypeptide (light green line), thus indicating a stronger impact on the barrier stability of hCMEC/D3. The histograms showed that the disturbance of the monolayer integrity progressed over time when deposition at 10 and 20 hours was compared (data are representative of one representative experiment performed in quadruplicate out of three independent assays, Fig. 8B, top histogram). Drops in the CI are given by the slopes of the curves and they correlated with the extent of CI changes because cells expressing Myc-WH2 and Myc-Spire-1 displayed the highest values (Fig. 8B, bottom histogram). Finally, monitoring of cells overexpressing Myc-Spire-1 or GFP-Spire-1 during the trans-migration process across VE-Cadherin-labeled monolayers confirmed that Spire-1 accumulated in dot-like spots that were preferentially located in the membrane expansions (Fig. 8C) that colocalized with actin-enriched sites (Fig. 8D, see higher magnifications in insets). Therefore, in our *in vitro* model, the rate and amplitude of the endothelium barrier destabilization are modulated by Spire-1 in invadosome-forming cells.

## DISCUSSION

The aggressiveness of cancer cells is characterized by their ability to invade across tissue boundaries, by breaching and degradation of ECM, navigation within the stroma and crossing the vasculature (Parekh et al., 2011). A gain of invasive activity can reflect a vast panoply of structural and regulatory changes depending on cell and tissue types, but they most often converge on an increase in the motile properties of cells. Such an increase is commonly associated with the acquisition of specialized mechano-sensitive structures that are actin-rich, finger-like cellular protrusions or invadosomes (Murphy and Courtneidge, 2011). In addition to driving motile behavior, these appendages are also sites towards which proteolytic enzymes traffic and are then released to degrade ECM locally (Linder et al., 2011).

A recent comprehensive proteomic-based analysis applied to 'invadosome-like' macrophages has unveiled the complexity of their architecture. Strikingly, among the 203 components identified, 170 are new structural and regulatory members largely composed of cytoskeleton proteins, GTP-binding and GTPase factors (Cervero et al., 2012). Invadosome scaffolding relies on actin nucleation, with a tight cooperation between the Arp2/3

Journal of Cell Science (2014) 127, 328–340 doi:10.1242/jcs.130161

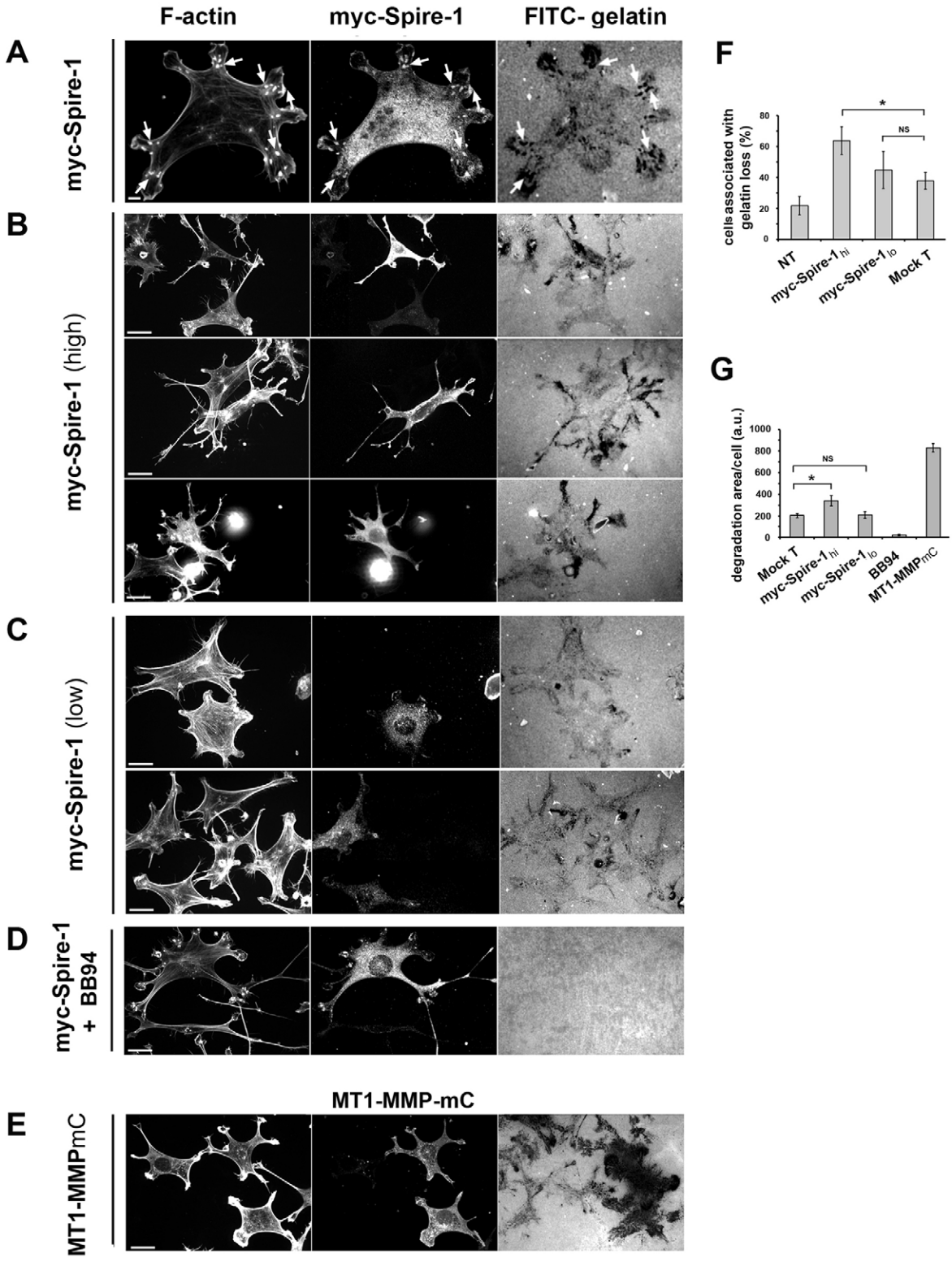


**Fig. 7. Overexpression of Spire-1 in 3T3 Src$^{+}$ cells increases gelatin matrix degradation.** (A–E) 20 hours post transfection with the Myc-Spire-1 (A–D) or MT1-MMPmC (E) encoding plasmids, $6\times10^{4}$ 3T3-Src$^{+}$ cells were deposited on top of a thin layer of a FITC-gelatin and cultured for 6 hours (A–C) or in the presence of 10 μM of the MMP inhibitor BB94 (D). Cells were stained with anti-Myc antibodies and fluorescent Phalloidin (A–D). White arrows indicate Spire-1 and F-actin-positive invadosomes and the corresponding matrix degraded spots (A). Selected frames of cells expressing high (B) or low (C) levels of Myc-Spire-1 juxtaposed with cells expressing no detectable protein are shown with the corresponding gelatin-degradation area. Note the absence of digested gelatin area for cells treated with BB94 (D) that strikingly contrasts with the large loss of gelatin area seen for cells overexpressing MT1-MMPmC (E). Scale bars: 10 μm. (F,G) Histograms show the percentage of cells ($n=50$) that associated with matrix digested area (F) and the index of matrix degradation (G) for different categories of cells including non-transfected cells (NT), mock (mock T) and Myc-Spire-1 (hi, high; lo, low) transfected cells. Statistical analyses were performed using the Student's *t*-test, *$P<0.05$; NS, not significant.

Journal of Cell Science (2014) 127, 328–340 doi:10.1242/jcs.130161

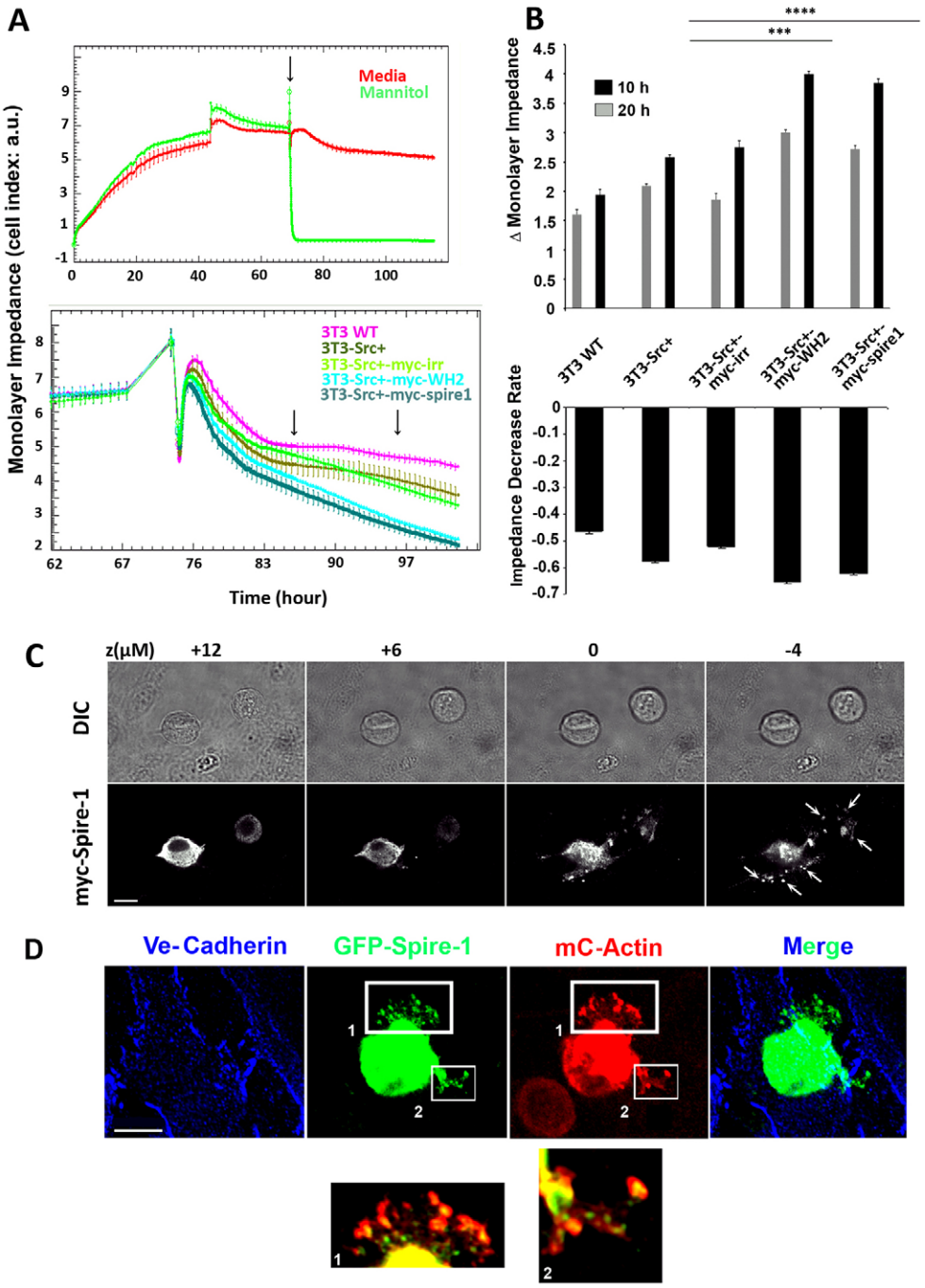


**Fig. 8. Overexpression of Myc-Spire-1 associates with an increase in the invasive properties of 3T3-Src$^{+}$ cells.** (A) Graphs showing cell index (CI, arbitrary units, a.u.) for hCMEC/D3 cells grown to confluency using the *xCELLigence* RTCA device. When a CI of about 7 was stabilized, change in culture medium or addition of mannitol, which disrupts cell tight junctions (arrows), led to slight or drastic changes in impedance, respectively (top graph). Addition of 3T3-WT (pink), 3T3-Src$^{+}$ (dark green), 3T3-Src$^{+}$ expressing Myc-Spire-1 (dark blue), 3T3-Src$^{+}$ expressing Spire-1-WH2 domain (light blue) and 3T3-Src$^{+}$ expressing irrelevant Myc fusion protein (light green) disturbs barrier function to variable extents over time (Fig. 8A, bottom graphs). (B) The histograms recapitulate the disturbance caused on monolayer integrity by addition of cell populations at 10 and 20 hours after cell deposition (top histogram) and the rate in CI decrease (bottom histogram). Data are representative of one representative experiment performed in quadruplicates out of three independent assays). ***$P<0.01$; ****$P<0.001$. (C,D) Cells overexpressing Myc-Spire-1 (C) or both GFP-Spire-1 and mCherry-actin (mC-actin) (D) are trans-migrating across an endothelial monolayer stained (D) using anti-VE-cadherin antibodies to visualize tight junctions between adjacent cells. Confocal *z* planes are indicated; DIC (top panel in C) and fluorescent (bottom panel in C, and D) images show Myc-Spire-1 and GFP-Spire-1 at the membrane extensions (white arrows, C). Note that the peripheral GFP-Spire-1 dots colocalize with mC-actin (D), zoomed images of merge framed areas 1 and 2, bottom panels). Scale bars: 10 μm.

actin-nucleating complex and the class of formins. For instance, a sixfold increase in FRL1 formin expression accompanies differentiation of human peripheral blood monocytes in macrophages (PBMCs) with preferential protein localization at the actin core of podosomes (Mersich et al., 2010). Full competence of invadosome proteolytic activities was also shown to depend on the formins present in cancer cells (Lizárraga et al., 2009). The present study enlarges the contribution of actin nucleators to invadosome biology with the identification of Spire-1 as the third nucleator type to add to the list. First, we found that Spire-1 was expressed and recruited to individual and clustered invadosomes in Src-transformed cells. The participation of Spire-1 to a molecular complex containing the formin mDia1, but not Arp2/3, together with the presence of formin in a cap layering the actin-Arp2/3 core (Mersich et al., 2010) support a selective interplay between different actin nucleators to the multipartite architecture of invadosomes. Spire has already been shown to function in cooperation with either the Arp2/3 complex and more frequently with formins to drive vesicular movement during the endocytic and exocytic pathways (Morel et al., 2009; Schuh, 2011). Interestingly, our study seems to indicate that the mDia1-Spire1 partnership occurs at invadosomes without ruling out the possibilities that other members of the broad formin family also act as partners of Spire-1 along the exocytic pathway. Regulatory interactions between the FH2 domain of the Cappuccino family formin (or the formin 2, Fmn2) and the Spire KIND domain have been identified *in vitro* and *in vivo* (Quinlan et al., 2007). Because we identified Spire-1and mDia-1 within the

same complex in $Src^+$ cells and probably also at the invadosomes, it will be of further interest to decipher whether the formin also activates Spire-1 nucleation activity in these sites.

Following the discovery of Spire-1 at invadosome sites, we next assessed whether Spire-1 contributes to invadosome functions by analysing the impact of Spire expression level on two of their main properties: ECM degradation and breach of the tissue or cellular barrier. First, using gelatin-degradation assays, we showed a moderate decrease of cell proteolytic activity when Spire-1 expression was lowered by RNA interference and a reciprocal increase when cells overexpressed Spire-1. Second, we monitored in real time the effect of overexpression of Spire-1 on the ability of cells to invade endothelial barriers and found that overexpressing Spire-1 speeded up and increased the extent of endothelial monolayer invasion. Of note, because we relied on cells with transfection rates varying between 40% and 50%, our data might under-report the real impact of Spire-1 on the invasiveness of $Src^+$ cells towards endothelia.

These functional data unveil a contribution of Spire-1 during ECM lysis and vessel breaching. In line with this, we detected Spire-1 localized as dots closely juxtaposed to F-actin in membrane expansions of cells crossing endothelia. In addition, Spire-1 and the *Drosophila* p150 Spire were proposed to act at the secretory pathway controlling Golgi vesicular trafficking in 3T3-WT fibroblasts that do not form invadosomes, through a possible connection with Rab11 with which exogenous p150-Spire colocalizes (Kerkhoff et al., 2001; Schuh, 2011). Moreover, a close spatial relationship between cancer cell invadopodia and the Golgi has been already reported (Buxione et al., 2004). In support of the involvement of Spire-1 in the secretion of lytic enzymes at invadosome sites, we found that modulation of Spire-1 expression affects their digestive potency. Pro-invasive activities of MMPs require their targeting to invadosomes, a process that is expected to be driven by a combinatory set of Rab GTPases and effectors that still need to be characterized in detail. Interestingly, Rab27A, which is defined as a functional partner of Rab3A, has been associated with the invasive and metastatic potential of breast cancer cells, because it promotes the expression of several proteases involved in breaching of the ECM (Tedone et al., 1997). Rab3A has also been directly involved in regulated exocytosis in several cell types, including those switching to aggressive tumor cell behavior. Our study uncovers a novel partnership between Rab3A and Spire-1 at the invadosome sites and this finding fits with the concomitant upregulation of both proteins in $Src^+$ cells. The selective implication of the Spire-1 C-terminal domain in the interaction with Rab3A might explain why the Spire-1 N-KIND domain, when expressed alone does not follow a typical dot-like distribution (Fig. 3; supplementary material Fig. S3). Collectively, these results are consistent with a role for Spire-1 in vesicular trafficking of lytic products through the secretory or exocytic pathway. If the Rab3 and Spire-1 partnership promotes the polarized vesicular traffic of MMPs to invadosomes, other Rab proteins, in particular Rab8, which are known to regulate MMP traffic and exocytosis (Bravo-Cordero et al., 2007) are likely to be part of the process as well. Remarkably, we observed a strong association between Rab8A and Spire-1 vesicles in the cytoplasm of $Src^+$ fibroblasts, whereas at the invadosome sites, the membrane-associated MT-MMP1 was clearly seen at the membranous edges and Myc-Spire-1 remained coincident with the F-actin-enriched invadosomes. These observations suggest that Spire-1 might indeed be important for invadosome structure and function (supplementary material Fig. S6B). Future work should aim to assess whether and how Spire-1 contributes to the scaffolding of invadosomes.

In conclusion, our results newly support a cooperation of Spire-1 with other components to actin nucleation and vesicular traffic at the invadosome sites in cancer and transformed cells. In addition to supplying invadosomes with proteolytic products, exocytosis of Spire-1-positive vesicles could also provide membrane material to fold these growing protrusive devices and it will be of interest to assess the contribution of Spire-1 to matrix or tissue invasion under 3D conditions. Future studies should aim to decipher the interplay between the different classes of actin nucleator. This would lead to an understanding of the control of vesicular trafficking and docking of enzymes at invadosomes or protrusive invasive pseudopods whose activities accompany numerous physiological and pathophysiological processes, most importantly cancer metastasis.

## MATERIALS AND METHODS

### Cell culture

Culture media and reagents were purchased from Gibco, Life Technologies (Saint Aubin, France) unless specified. Human embryonic kidney cells (HEK-293) and MDA-MB-231 breast adenocarcinoma cells, mouse embryonic fibroblasts (NIH3T3) WT and stably expressing active Src ($Src^+$) cells and pre-osteoclasts stably expressing active Src were grown in Dulbecco's minimum essential medium (DMEM) supplemented with glutamax, 10% heat-inactivated fetal bovine serum, penicillin (100 U/ml), streptomycin (100 µg/ml) and 10 mM HEPES. Human brain endothelial cells (HCMEC/D3) were grown in EBM-2 medium supplemented as described (Luissint et al., 2012; Lonza, Verbiers, Belgium). Cells were cultured at 37℃ under 95% $O_2$ and 5% $CO_2$.

### RT-PCR to detect *Spire1* transcripts in different cell lines

RNA was extracted using the RNeasy Mini Kit (Qiagen, Courtaboeuf, France) according to the supplier's instructions. For cDNA synthesis 2.5 µg of total RNA were retro-transcribed using the SuperScript kit (Invitrogen Life Technologies). For control reactions, 2.5 µg of RNA was treated without reverse transcriptase. PCR was performed with NEB Taq Polymerase in a 25 µl final volume containing 1/10th cDNA volume, 0.2 µM of primers and 200 µM of DNTPs. The integrity of cDNA was checked by amplification of the housekeeping gene *Arp3*, and *Spire1* transcripts were detected with specific primers targeting mouse *Spire1* but not *Spire2* genes (all primers are listed in supplementary material Table S1). Integrity of the PCR products was controlled by nucleotide sequencing before further analysis.

### Western blot analysis of Spire-1 and Rab3A

Whole-cell extracts ranging from $5\times10^4$ to $5\times10^5$ cells or protein lysates (15–50 µg) were analyzed by SDS-PAGE and western blotting. Nitrocellulose membranes were probed with appropriate primary (supplementary material Table S2) and secondary HRP-coupled antibodies (Pierce Fisher Scientific, Illkirch, France). Chemiluminescent signals were scanned and quantified using ImageJ software (W. Rasband, NIH, Bethesda, MD) and normalized to GAPDH signals.

### Cloning procedures

The plasmid pCDNA3-Myc *Spire1* was used as a template to amplify the different regions of interest: full length Spire-1, the region encompassing the four WH2 domains (268–480aa) and the Cter (556–756aa); WH2-Cter (268–756aa), N-KIND (1–230aa) and N-KIND-WH2 (1–460aa) domains were amplified with appropriate primers. Fragments were further cloned in pEGFP-C3 (Spire-1) or in pCS2-Myc (domains) plasmids. The C-terminal domain was also cloned in pCS2-HA plasmid. For affinity pull-down assay, a GST-WH2 recombinant polypeptide was cloned in the pGex6-p3 vector. For interaction assays, N-KIND (1–230aa) and C-terminal (389–756aa) domains were amplified and cloned in the pET2817 plasmid modified to express a His-GST tag in N-terminal part of the fusion protein (pET2817-hGST, from S. Bellais, Institut Cochin, Paris). The PCR fragments were inserted in the PET2817-hGST plasmid using the In-Fusion HD cloning kit (Takara Bio/Clontech)

following manufacturer's instructions. Primers also encompassed *Nco*I and *Bam*HI sites for positive clone screening. Corresponding primers are listed in supplementary material Table S1.

### Cell transfection

Transfections were performed with the JetPei reagent (Polyplus, Illkirch, France) for HEK-293 cells, with Lipofectamine LTX (Invitrogen Life Technologies) for MDA-MB-231 and pre-osteoclast-Src$^+$ cells and with the Neon® Transfection System (Invitrogen Life Technologies) for 3T3-Src$^+$ cells (1200 V, 20 ms, three pulses). In all experiments, cells were cultivated for ~24 hours in complete medium before further analysis. For silencing experiments, MDA-MB-231 cells were treated with small interfering RNAs targeting *Spire1* (pool of three siRNA AMBION s32366, s32367 and s32368, 30 nM each) or with 100 nM of siRNA targeting *cortactin* (Sauvonnet et al., 2005) (Eurogenetc) or with 50 nM of AllStars Negative Control siRNA (Qiagen, Courtaboeuf, France). Two rounds of transfection were performed using the transfection agent Lipofectamine® RNAiMAX™ (Invitrogen, Lifetechnologies) 24 hours and 72 hours after passaging, respectively. At 24 hours post silencing transfection, cells were transfected using Lipofectamine LTX (Invitrogen Life Technologies) to ectopically express a MT1-MMP-mCherry fusion protein.

### Immunostaining, microscopy and image analysis

Cells were fixed in 4% paraformaldehyde (20 minutes, 23℃), permeabilized in 0.5% (v/v) Triton X-100 (TX-100, 5 minutes, 23℃) and incubated in PBS with 2% (w/v) BSA (20 minutes, 23℃) before adding the appropriate primary and Alexa-Fluor-coupled secondary antibodies (supplementary material Table S2) or Alexa Fluor Phalloidin (Invitrogen Life Technologies). In some assays, nuclei were stained with 4′,6-diamidino-2-phenylindole (DAPI). Cells were observed under a confocal microscope (Eclipse T*i* Nikon). Image stacks were acquired with a 14-bit Cool SNAP HQ camera (Roper Scientific, Lisses, France) under Metamorph software (Universal Imaging Corporation) and further processed with ImageJ and Adobe R Adobe Photoshop software. Maximal projections are shown in Figures.

### Immunopurification of the Spire-1 complex

$10^6$ 3T3-Src$^+$ cells ectopically expressing Myc-Spire-1 were solubilized in lysis buffer A and centrifuged (20,000 ***g***, 20 minutes, 4℃). Supernatants were incubated with anti-Myc agarose beads (Sigma-Aldrich, St Quentin Fallaviers, France) (2 hours, 4℃) before extensive washing. Bound proteins were eluted in 50 µl of SDS sample buffer, DTT (25 mM) was added and samples were subjected to SDS-PAGE. Proteins were transferred to nitrocellulose membranes before western blotting with appropriate antibodies (supplementary material Table S2). GAPDH was used as a control of specificity. Similar protocols were applied to investigate Myc-Spire-1 partnerships with GFP-Rab3A starting with 3T3-Src$^+$ cells co-transfected with Myc-Spire-1 and GFP-Rab3A or GFP-Rab5A.

### *In vitro* interaction assays

Recombinant GST-WH2 and GST proteins were produced in BL21*(DE3)pLysS E. coli* strain (2 hours, 37℃ 0.1 mM isopropyl β-D-1-thiogalactopyranoside (IPTG), Euromedex, Souffelweyrsheim, France). Bacteria were solubilized in buffer B supplemented with 0.5% TX-100 (30 minutes, 4℃). After centrifugation (43,000 ***g***, 10 minutes, 4℃), supernatants were incubated with glutathione-Sepharose C4B beads (Ge Healthcare, Strasbourg, France) (2 hours, 4℃). Beads were washed with buffer B supplemented with 0.01% TX-100 and subsequently equilibrated in buffer C. HEK-293 cells expressing Myc-Spire-1, Myc-KIND or HA-C-terminal fusion polypeptides were solubilized in buffer C supplemented with 0.1% TX-100 (20 minutes, 4℃) and lysates were centrifuged (20,000 ***g***, 20 minutes, 4℃). Half of the supernatant was incubated with immobilized GST-WH2 and the other half with immobilized GST (2 hours, 4℃). Beads were spun down (1000 ***g***, 5 minutes, 4℃) and unbound products were eliminated with buffer C containing 0.01% TX-100. Bound proteins were eluted in 40 µl of SDS-sample buffer containing DTT and analyzed by SDS-PAGE and western blot using appropriate antibodies (supplementary material Table S2). Recombinant GST-Rab3A proteins were produced in the Rosetta BL21 *E. coli* strain (5 hours, 37℃, 0.5 mM IPTG). Bacteria were resuspended in buffer D and treated as described above with the addition of 1 µM of GTP prior and during the interaction assay. HEK-293 cells were collected in buffer E, ruptured with liquid nitrogen and incubated on ice (20 minutes). After centrifugation, lysates were incubated with immobilized GST or GST-Rab3A (2 hours, 4℃) unbound proteins were eliminated whereas bound proteins were analyzed by SDS-PAGE and western blotting (supplementary material Table S2). *In vitro* assays were conducted with 5 µg of recombinant protein immobilized on nickel beads and further incubated with 5 µg of pre-dialyzed GST-WH2 domains in a final volume of 100 µl of buffer B supplemented with 0.02% of TX-100 (2 hours, 4℃). Following elimination of unbound material, eluates were recovered in SDS-PAGE sample buffer containing DTT and further analyzed by SDS-PAGE and western blotting.

### Gelatin-degradation assay

Gelatin-degradation assays were performed as described previously (Artym et al., 2006). $6\times10^4$ 3T3-Src$^+$ cells either mock transfected or transfected with either Myc-Spire-1 or MT1-MMP-mCherry plasmids were plated 20 hours post transfection on the gelatin layer covering a 18 mm glass coverlisp and cultured in DMEM containing 0.2% FBS (6 hours, 37℃) before immunostaining. In some experiments, 3T3-Src$^+$ cells expressing Myc-Spire-1 were exposed to the metalloprotease inhibitor, batimastat (BB94, 10 µM) over the assay period. Matrix degradation was assessed by quantifying (1) the number of cells associated with degradation and (2) the local area of loss of fluorescence with respect to cells (~50 cells for each transgene expression and/or treatment; two independent experiments). A similar protocol was applied to silenced MDA-MB-231 cells ($10^5$ on gelatin-coated coverslips). The extent of matrix degradation was assessed by quantifying fluorescence loss with respect to cell area (~40 MT1-MMP-mCherry-expressing cells for each siRNA treatment; two independent experiments). Merged image stacks were analyzed using ImageJ software and statistical analyses were performed using the Student's *t*-test.

### Transmigration assays on endothelial barrier

To monitor cell invasion through a monolayer of HCMEC/D3 cells, we used the impedance-based *xCELLigence* Real-Time Cell Analysis detection technology (Roche Applied Science). Invasion experiments were carried out in 96-well microplates in a humidified incubator at 37℃ and 5% $CO_2$ and data were recorded with the RTCA software (versus 1.2.1). First, *xCELLigence* E-plates 96 (Roche) were coated with 0.1% gelatin (1 hour, 37℃) and filled with medium to measure background impedance in the absence of cells. Then, $1.5\times10^4$ HCMEC/D3 cells were seeded per well and grown until they formed a monolayer and reached a plateau of maximal cell index values. Medium was changed after 48 hours of culture. When the plateau was stabilized, single-cell suspensions of $1.5\times10^4$ 3T3-WT or -Src$^+$ cells transfected 20 hours before with plasmids encoding irrelevant Myc-polypeptide, Myc-Spire-1 or Myc-Spire-1 domains were deposited on top of the monolayer in 10% FBS DMEM medium. Monolayer disturbance during cell invasion was recorded over a period of 30 hours (every 5 minutes for the first 2 hours, every 15 minutes for next 2 hours and every 30 minutes for the remaining period). To catch the trans-migration process, the assay was performed with ten times more 3T3-Src$^+$ cells expressing both GFP-Spire-1 and mCherry-actin and cells were fixed for immunofluorescence labeling (VE-Cadherin) after 4 hours of contact.

#### Acknowledgements

We thank S. Courtneige (La Jolla, CA) and F. Saltel (Bordeaux, France) for providing us with the NIH 3T3 cells. We are grateful to P. Chavrier for giving us the MT1-MMPmCherry plasmid, the MDA-MB231 cell line and numerous helpful advice for the gelatin-degradation assay. We thank M.R. Block (Grenoble, France) for the gift of pre-osteoclasts stably expressing activated Src kinase and E. Kerkhoff (Regensburg, Germany) for kindly providing us with the Myc Spir-1 plasmid. We thank R. Regazzi (Lausanne, Switzerland) for providing GST-Rab3A and GFP-Rab3A plasmids and M. Fukuda (Tohoku, Japan) for the GFP-Rab5A plasmid, respectively. We are grateful to R.E. Pagano (Rochester, NY) for the gift of GFP-Rab7A and Rab11A plasmids and to M.V. Nachury (San Francisco, CA) for the GFP-Rab8A plasmid. We also thank G.M. Bokoch (La Jolla, CA) for the mCherry actin plasmid and V. Delorme-Walker (la Jolla, CA) for the careful reading of the manuscript.

**Competing interests**
The authors declare no competing financial interests.

**Author contributions**
V.L. and I.T. designed and performed the experiments, M.A., V.G., A.P., S.P. and E.V. performed experiments I.T. conceived this study; I.T. and V.L. wrote the manuscript.

**Funding**
Work was funded by the French Government Research Agency [grant number MIERPV08023KSA]; and the 'Fondation pour la Recherche Médicale' agency [grant number DEQ20100318279]. V.L. is a senior post-doctoral fellow financed by an EC Marie Curie integration grant [grant number PIRG05-GA-2009-249158] and the FRM [grant number DEQ20100318279]. The Nikon confocal imaging facilities were sponsored by the 'Domaines d'Intérêts Majeurs' DIM MALINF' [grant numbers R11042KK RPH11042KKA]; and FRM [grant number DEQ20100318279].

**Supplementary material**
Supplementary material available online at
http://jcs.biologists.org/lookup/suppl/doi:10.1242/jcs.130161/-/DC1

**References**

**Albiges-Rizo, C., Destaing, O., Fourcade, D., Planus, E. and Block, M. R.** (2009). Actin machinery and mechanosensitivity in invadopodia, podosomes and focal adhesions. *J. Cell Sci.* **122**, 3037-3049.
**Artym, V. V., Zhang, Y., Seillier-Moiseiwitsch, F., Yamada, K. M. and Mueller, S. C.** (2006). Dynamic interactions of cortactin and membrane type 1 matrix metalloproteinase at invadopodia: defining the stages of invadopodia formation and function. *Cancer Res.* **66**, 3034-3043.
**Baldini, G., Scherer, P. E. and Lodish, H. F.** (1995). Nonneuronal expression of Rab3A: induction during adipogenesis and association with different intracellular membranes than Rab3D. *Proc. Natl. Acad. Sci. USA* **92**, 4284-4288.
**Boateng, L. R., Cortesio, C. L. and Huttenlocher, A.** (2012). Src-mediated phosphorylation of mammalian Abp1 (DBNL) regulates podosome rosette formation in transformed fibroblasts. *J. Cell Sci.* **125**, 1329-1341.
**Bolte, S. and Cordelières, F. P.** (2006). A guided tour into subcellular colocalization analysis in light microscopy. *J. Microsc.* **224**, 213-232.
**Bravo-Cordero, J. J., Marrero-Diaz, R., Megías, D., Genís, L., García-Grande, A., García, M. A., Arroyo, A. G. and Montoya, M. C.** (2007). MT1-MMP proinvasive activity is regulated by a novel Rab8-dependent exocytic pathway. *EMBO J.* **26**, 1499-1510.
**Buccione, R., Orth, J. and McNiven, M.** (2004). Foot and mouth: podosomes, invadopodia and circular dorsal ruffles. *Nat. Rev. Mol. Cell Biol.* **5**, 647-657.
**Bustos, M. A., Lucchesi, O., Ruete, M. C., Mayorga, L. S. and Tomes, C. N.** (2012). Rab27 and Rab3 sequentially regulate human sperm dense-core granule exocytosis. *Proc. Natl. Acad. Sci. USA* **109**, E2057-E2066.
**Caldieri, G. and Buccione, R.** (2010). Aiming for invadopodia: organizing polarized delivery at sites of invasion. *Trends Cell Biol.* **20**, 64-70.
**Cervero, P., Himmel, M., Krüger, M. and Linder, S.** (2012). Proteomic analysis of podosome fractions from macrophages reveals similarities to spreading initiation centres. *Eur. J. Cell Biol.* **91**, 908-922.
**Cougoule, C., Le Cabec, V., Poincloux, R., Al Saati, T., Mège, J. L., Tabouret, G., Lowell, C. A., Laviolette-Malirat, N. and Maridonneau-Parini, I.** (2010). Three-dimensional migration of macrophages requires Hck for podosome organization and extracellular matrix proteolysis. *Blood* **115**, 1444-1452.
**Destaing, O., Planus, E., Bouvard, D., Oddou, C., Badowski, C., Bossy, V., Raducanu, A., Fourcade, B., Albiges-Rizo, C. and Block, M. R.** (2010). β1A integrin is a master regulator of invadosome organization and function. *Mol. Biol. Cell* **21**, 4108-4119.
**Dovas, A., Gevrey, J. C., Grossi, A., Park, H., Abou-Kheir, W. and Cox, D.** (2009). Regulation of podosome dynamics by WASp phosphorylation: implication in matrix degradation and chemotaxis in macrophages. *J. Cell Sci.* **122**, 3873-3882.
**Egeblad, M. and Werb, Z.** (2002). New functions for the matrix metalloproteinases in cancer progression. *Nat. Rev. Cancer* **2**, 161-174.
**Firat-Karalar, E. N. and Welch, M. D.** (2011). New mechanisms and functions of actin nucleation. *Curr. Opin. Cell Biol.* **23**, 4-13.
**Ho, J. R., Chapeaublanc, E., Kirkwood, L., Nicolle, R., Benhamou, S., Lebret, T., Allory, Y., Southgate, J., Radvanyi, F. and Goud, B.** (2012). Deregulation of Rab and Rab effector genes in bladder cancer. *PLoS ONE* **7**, e39469.
**Ina, K., Kitamura, H., Tatsukawa, S., Miyazaki, T., Abe, H. and Fujikura, Y.** (2005). Intracellular formation of collagen microfibrils in granulation tissue. *Exp. Mol. Pathol.* **79**, 244-248.
**Irby, R. B. and Yeatman, T. J.** (2000). Role of Src expression and activation in human cancer. *Oncogene* **19**, 5636-5642.
**Kaksonen, M., Toret, C. P. and Drubin, D. G.** (2006). Harnessing actin dynamics for clathrin-mediated endocytosis. *Nat. Rev. Mol. Cell Biol.* **7**, 404-414.
**Kerkhoff, E.** (2006). Cellular functions of the Spir actin-nucleation factors. *Trends Cell Biol.* **16**, 477-483.
**Kerkhoff, E., Simpson, J. C., Leberfinger, C. B., Otto, I. M., Doerks, T., Bork, P., Rapp, U. R., Raabe, T. and Pepperkok, R.** (2001). The Spir actin organizers are involved in vesicle transport processes. *Curr. Biol.* **11**, 1963-1968.
**Lankat-Buttgereit, B., Fehmann, H. C., Hering, B. J., Bretzel, R. G. and Göke, B.** (1994). Expression of the ras-related rab3a gene in human insulinomas and normal human pancreatic islets. *Pancreas* **9**, 434-438.
**Linder, S.** (2007). The matrix corroded: podosomes and invadopodia in extracellular matrix degradation. *Trends Cell Biol.* **17**, 107-117.
**Linder, S., Wiesner, C. and Himmel, M.** (2011). Degrading devices: invadosomes in proteolytic cell invasion. *Annu. Rev. Cell Dev. Biol.* **27**, 185-211.
**Lizárraga, F., Poincloux, R., Romao, M., Montagnac, G., Le Dez, G., Bonne, I., Rigaill, G., Raposo, G. and Chavrier, P.** (2009). Diaphanous-related formins are required for invadopodia formation and invasion of breast tumor cells. *Cancer Res.* **69**, 2792-2800.
**Luissint, A. C., Artus, C., Glacial, F., Ganeshamoorthy, K. and Couraud, P. O.** (2012). Tight junctions at the blood brain barrier: physiological architecture and disease-associated dysregulation. *Fluids Barriers CNS.* **9**, 23.
**Mersich, A. T., Miller, M. R., Chkourko, H. and Blystone, S. D.** (2010). The formin FRL1 (FMNL1) is an essential component of macrophage podosomes. *Cytoskeleton (Hoboken)* **67**, 573-585.
**Leenders, A. G., Lopes da Silva, F. H., Ghijsen, W. E. J. M. and Verhage, M.** (2001). Rab3a is involved in transport of synaptic vesicles to the active zone in mouse brain nerve terminals. *Mol. Biol. Cell* **12**, 3095-3102.
**Morel, E., Parton, R. G. and Gruenberg, J.** (2009). Annexin A2-dependent polymerization of actin mediates endosome biogenesis. *Dev. Cell* **16**, 445-457.
**Murphy, D. A. and Courtneidge, S. A.** (2011). The 'ins' and 'outs' of podosomes and invadopodia: characteristics, formation and function. *Nat. Rev. Mol. Cell Biol.* **12**, 413-426.
**Parekh, A., Ruppender, N. S., Branch, K. M., Sewell-Loftin, M. K., Lin, J., Boyer, P. D., Candiello, J. E., Merryman, W. D., Guelcher, S. A. and Weaver, A. M.** (2011). Sensing and modulation of invadopodia across a wide range of rigidities. *Biophys. J.* **100**, 573-582.
**Parekh, A. and Weaver, A. M.** (2009). Regulation of cancer invasiveness by the physical extracellular matrix environment. *Cell Adh. Migr.* **3**, 288-292.
**Pavlos, N. J., Grønborg, M., Riedel, D., Chua, J. J., Boyken, J., Kloepper, T. H., Urlaub, H., Rizzoli, S. O. and Jahn, R.** (2010). Quantitative analysis of synaptic vesicle Rabs uncovers distinct yet overlapping roles for Rab3a and Rab27b in Ca2+-triggered exocytosis. *J. Neurosci.* **30**, 13441-13453.
**Pfender, S., Kuznetsov, V., Pleiser, S., Kerkhoff, E. and Schuh, M.** (2011). Spire-type actin nucleators cooperate with Formin-2 to drive asymmetric oocyte division. *Curr. Biol.* **21**, 955-960.
**Quinlan, M. E., Heuser, J. E., Kerkhoff, E. and Mullins, R. D.** (2005). Drosophila Spire is an actin nucleation factor. *Nature* **433**, 382-388.
**Quinlan, M. E., Hilgert, S., Bedrossian, A., Mullins, R. D. and Kerkhoff, E.** (2007). Regulatory interactions between two actin nucleators, Spire and Cappuccino. *J. Cell Biol.* **179**, 117-128.
**Renault, L., Bugyi, B. and Carlier, M. F.** (2008). Spire and Cordon-bleu: multifunctional regulators of actin dynamics. *Trends Cell Biol.* **18**, 494-504.
**Sabeh, F., Shimizu-Hirota, R. and Weiss, S. J.** (2009). Protease-dependent versus -independent cancer cell invasion programs: three-dimensional amoeboid movement revisited. *J. Cell Biol.* **185**, 11-19.
**Sauvonnet, N., Dujeancourt, A. and Dautry-Varsat, A.** (2005). Cortactin and dynamin are required for the clathrin-independent endocytosis of gammac cytokine receptor. *J. Cell Biol.* **168**, 155-163.
**Schuh, M.** (2011). An actin-dependent mechanism for long-range vesicle transport. *Nat. Cell Biol.* **13**, 1431-1436.
**Sibony-Benyamini, H. and Gil-Henn, H.** (2012). Invadopodia: the leading force. *Eur. J. Cell Biol.* **91**, 896-901.
**Soldati, T. and Schliwa, M.** (2006). Powering membrane traffic in endocytosis and recycling. *Nat. Rev. Mol. Cell Biol.* **7**, 897-908.
**Steffen, A., Le Dez, G., Poincloux, R., Recchi, C., Nassoy, P., Rottner, K., Galli, T. and Chavrier, P.** (2008). MT1-MMP-dependent invasion is regulated by TI-VAMP/VAMP7. *Curr. Biol.* **18**, 926-931.
**Tarone, G., Cirillo, D., Giancotti, F. G., Comoglio, P. M. and Marchisio, P. C.** (1985). Rous sarcoma virus-transformed fibroblasts adhere primarily at discrete protrusions of the ventral membrane called podosomes. *Exp. Cell Res.* **159**, 141-157.
**Tedone, T., Correale, M., Barbarossa, G., Casavola, V., Paradiso, A. and Reshkin, S. J.** (1997). Release of the aspartyl protease cathepsin D is associated with and facilitates human breast cancer cell invasion. *FASEB J.* **11**, 785-792.
**Vadlamudi, R. K., Wang, R. A., Talukder, A. H., Adam, L., Johnson, R. and Kumar, R.** (2000). Evidence of Rab3A expression, regulation of vesicle trafficking, and cellular secretion in response to heregulin in mammary epithelial cells. *Mol. Cell. Biol.* **20**, 9092-9101.
**Vizcarra, C. L., Kreutz, B., Rodal, A. A., Toms, A. V., Lu, J., Zheng, W., Quinlan, M. E. and Eck, M. J.** (2011). Structure and function of the interacting domains of Spire and Fmn-family formins. *Proc. Natl. Acad. Sci. USA* **108**, 11884-11889.
**Weaver, A. M.** (2008). Invadopodia. *Curr. Biol.* **18**, R362-R364.
**Weksler, B. B., Subileau, E. A., Perrière, N., Charneau, P., Holloway, K., Leveque, M., Tricoire-Leignel, H., Nicotra, A., Bourdoulous, S., Turowski, P. et al.** (2005). Blood-brain barrier-specific properties of a human adult brain endothelial cell line. *FASEB J.* **19**, 1872-1874.
**Wiesner, C., El Azzouzi, K. and Linder, S.** (2013). A specific subset of RabGTPases controls cell surface exposure of MT1-MMP, extracellular matrix degradation and three-dimensional invasion of macrophages. *J. Cell Sci.* **126**, 2820-2833.
**Wolf, K. and Friedl, P.** (2011). Extracellular matrix determinants of proteolytic and non-proteolytic cell migration. *Trends Cell Biol.* **21**, 736-744.
**Yu, X., Zech, T., McDonald, L., Gonzalez, E. G., Li, A., Macpherson, I., Schwarz, J. P., Spence, H., Futó, K., Timpson, P. et al.** (2012). N-WASP coordinates the delivery and F-actin-mediated capture of MT1-MMP at invasive pseudopods. *J. Cell Biol.* **199**, 527-544.

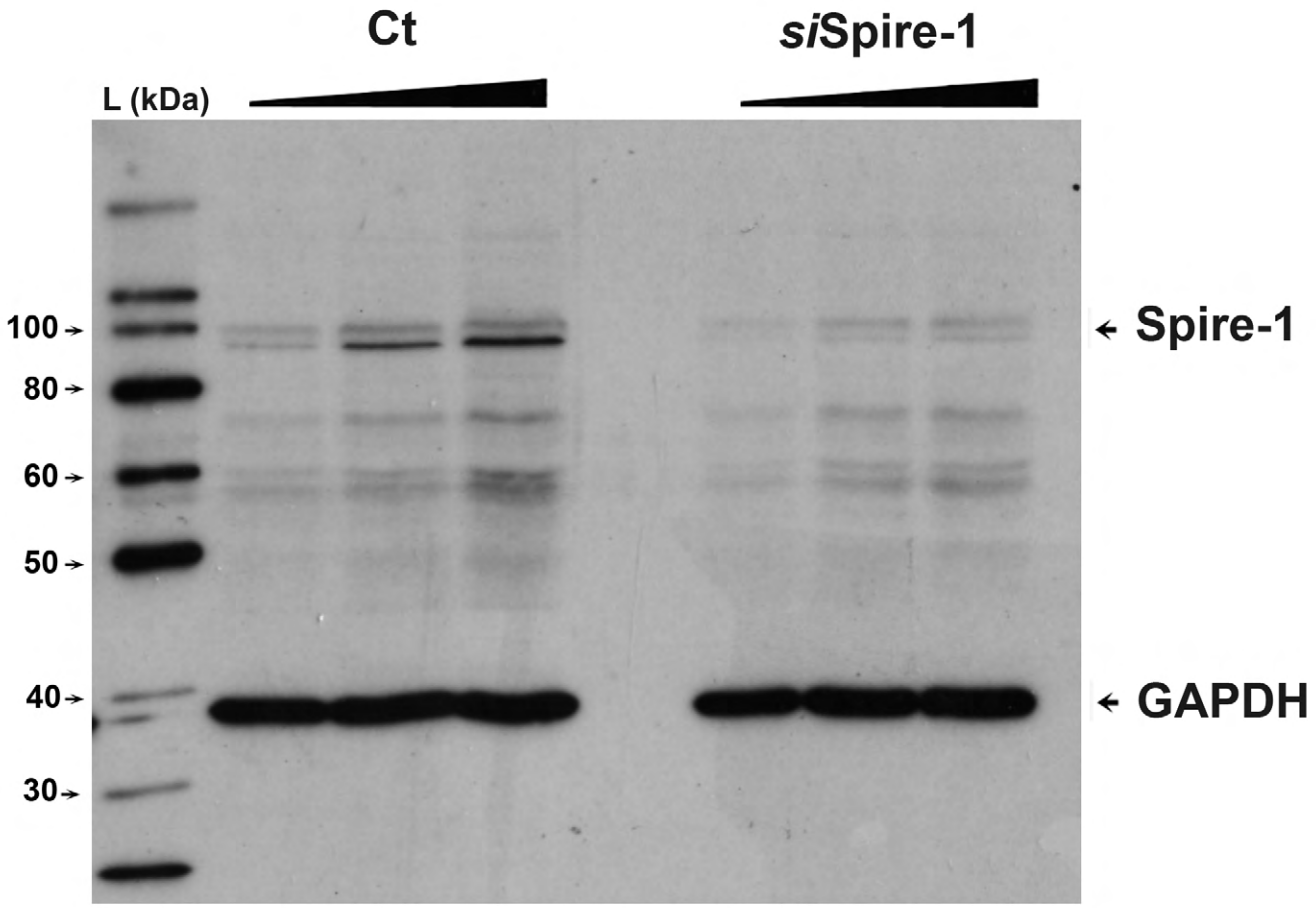


**Fig. S1. Western blot on whole cell extracts from $5x10^4$ to $5x10^5$ HEK-293 cells transfected with AllStars Negative Control siRNA (Qiagen) (Ct) or with siSpire-1 oligonucleotides (siSpire-1). The membrane was probed with the K19 anti-Spire-1 antibodies and anti-GAPDH antibodies. Note that K19 but not the GAPDH signal was significantly reduced in silenced cells. L: ladder (kDa).**

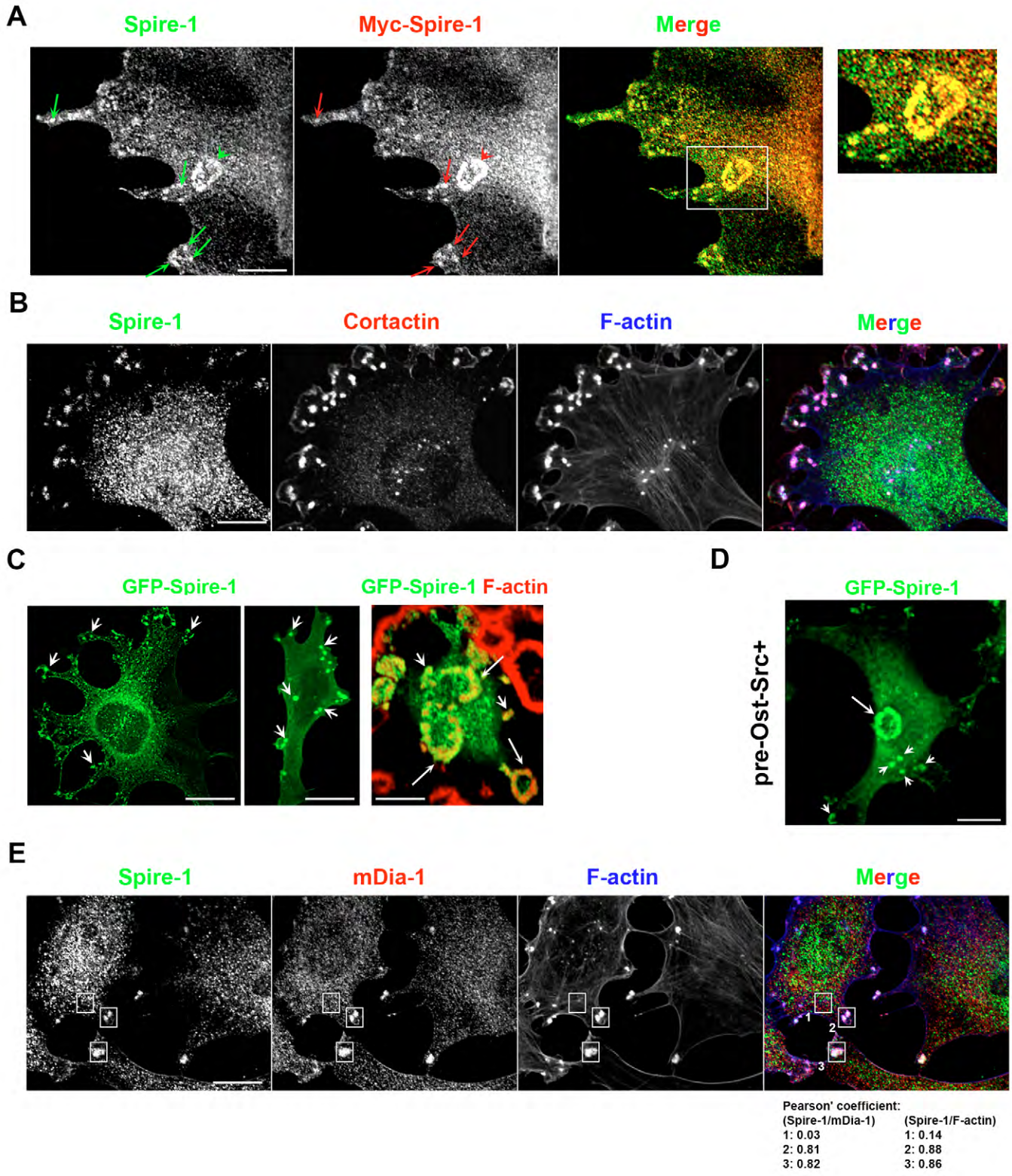


**Fig. S2. (A) Co-localization of endogenous Spire-1 and exogenous myc-Spire-1. 3T3-Src+ cells were stained with N-KIND-Spire-1 (green) and anti-myc (red) antibodies. Arrows and arrowheads show individual and clustered invadosomes, respectively. Framed area shown in the merge image is zoomed in right panel focusing on several invadosomes and a rosette. (B) Triple fluorescent labeling of 3T3-Src+ cells using N-KIND-Spire-1 (green) and Cortactin (red) antibodies and phalloidin (F-actin, blue); note the marked co-enrichment of the three proteins at invadosomes. (C,D) Transiently expressed GFP-Spire-1 (green) accumulates at F-actin enriched invadosomes in 3T3-Src+ (C) and in pre-Ost-Src+ (D) cells, short and long white arrows mark invadosomes and rosettes respectively (D). (E) Triple fluorescent labeling of 3T3-Src+ cells with N-KIND-Spire-1 (green) and anti-mDia1 (red) antibodies and with phalloidin to detect F-actin (blue); note that endogenous mDia1 and Spire-1 signals overlap only at invadosomes/rings sites as specified by the Pearson' co-localization coefficient. Scale bar: 10 µm.**

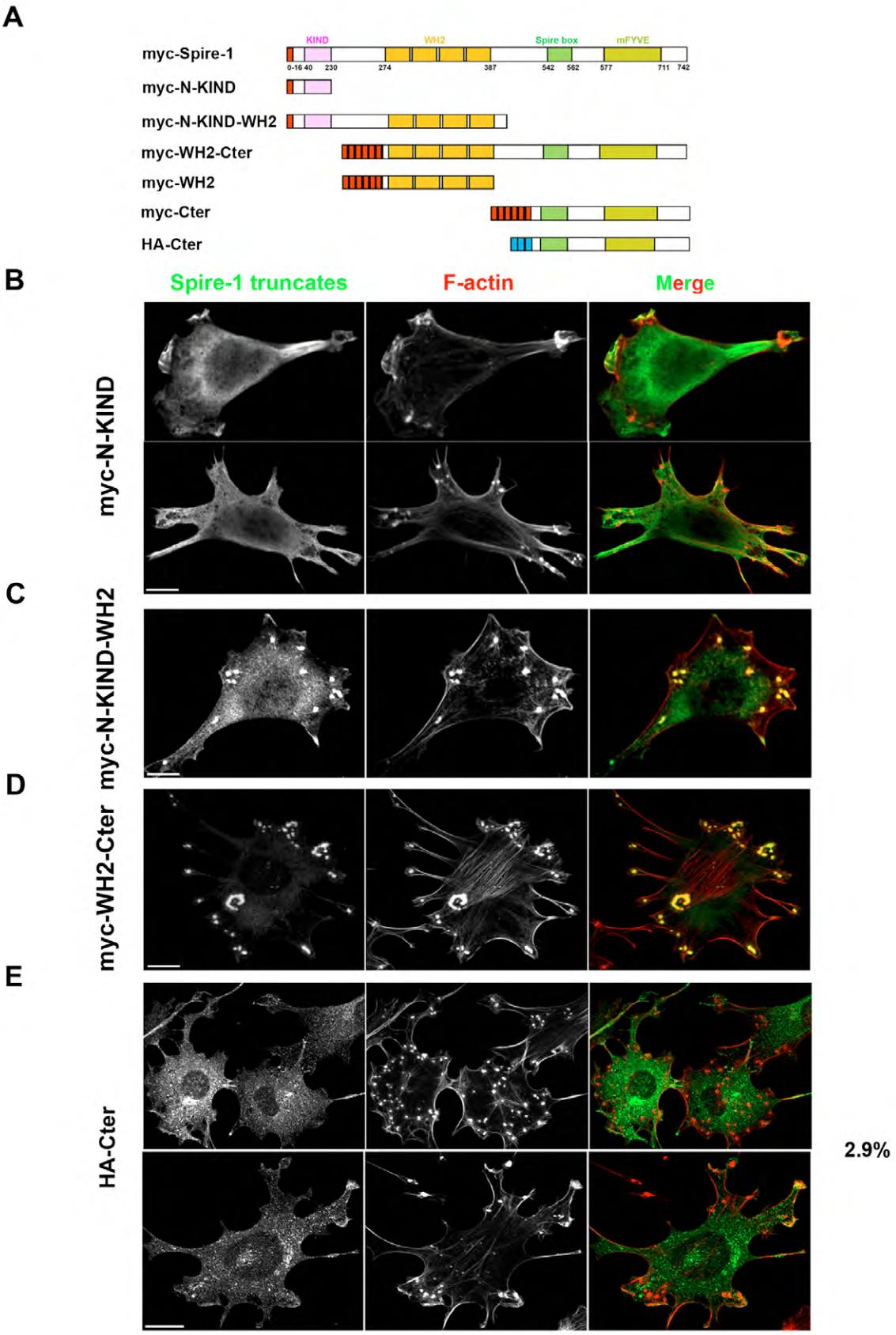


**Fig. S3. The Spire-1 WH2 domain drive Spire-1 to invadosomes. (A) Schematic representation of Spire-1 truncates in fusion with either myc (red boxes) or HA (blue boxes) tags engineered for mammalian expression. (B-E) 3T3-Src+ cells transiently expressing Spire-1 truncates in fusion with either myc (B-D) or HA (E) tags were labeled with anti-myc or anti-HA antibodies (green) and with phalloidin to detect F-actin (red). Note 27 the diffuse cytoplasmic staining together with some cell edge regions of myc-N-KIND (B) and the marked recruitment of myc-N-KIND-WH2 product to invadosomes (C). Note that myc-WH2-Cter accumulated at invadosomes (D) by contrast to the Spire-1 HA-Cter truncate (E), Scale bar: 10 µm.**

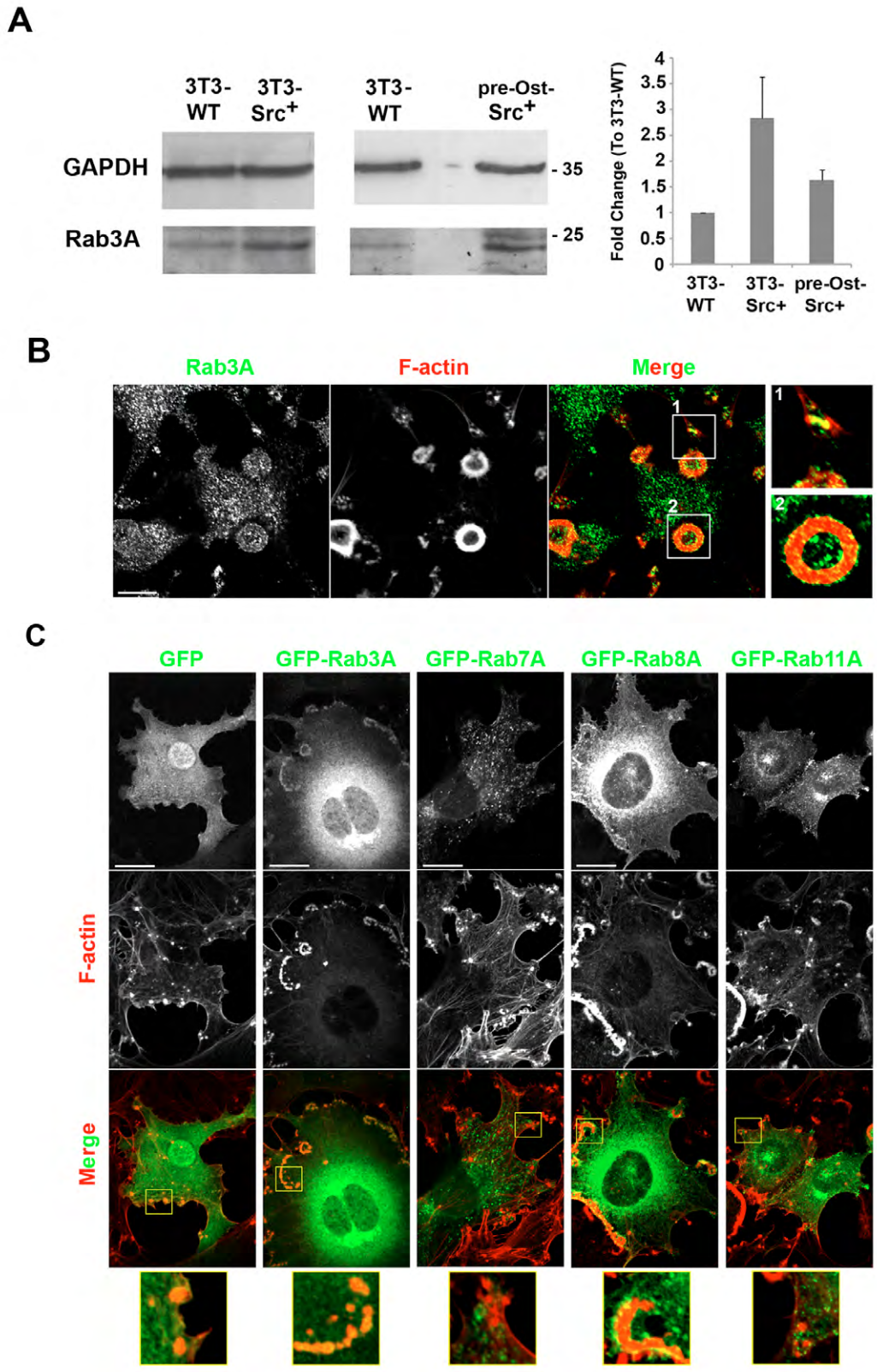


**Fig. S4. Rab3A is up-regulated in Src+ fibroblasts and pre-Osteoclasts and co-localizes with Spire-1-positive invadosomes and rings. (A) Whole cell extracts from 106 of 3T3-WT, 3T3-Src+ and pre-Osteoclast Src+ cells were analysed by Western blot using anti-Rab3A antibodies. Level of expression was quantified with ImageJ software using GAPDH protein as reference (Histograms, data are from 2 different cell extracts). Molecular weights are indicated in kDa. (B) 3T3-Src+ cells were stained with anti-Rab3A antibodies (green) and phalloidin to detect F-actin (red). Framed areas 1 and 2 in the merge image are zoomed in right panels 1 and 2. Note the enrichment of Rab3A-positive vesicles at invadosomes (frame 1) and at the ring (frame 2), scale bar: 10 µm. (C) 3T3-Src+ cells transiently expressing either GFP or GFP in fusion with different Rabs (green) as indicated were stained to detect F-actin (red). Framed areas are zoomed as additional insets below the corresponding panels.**

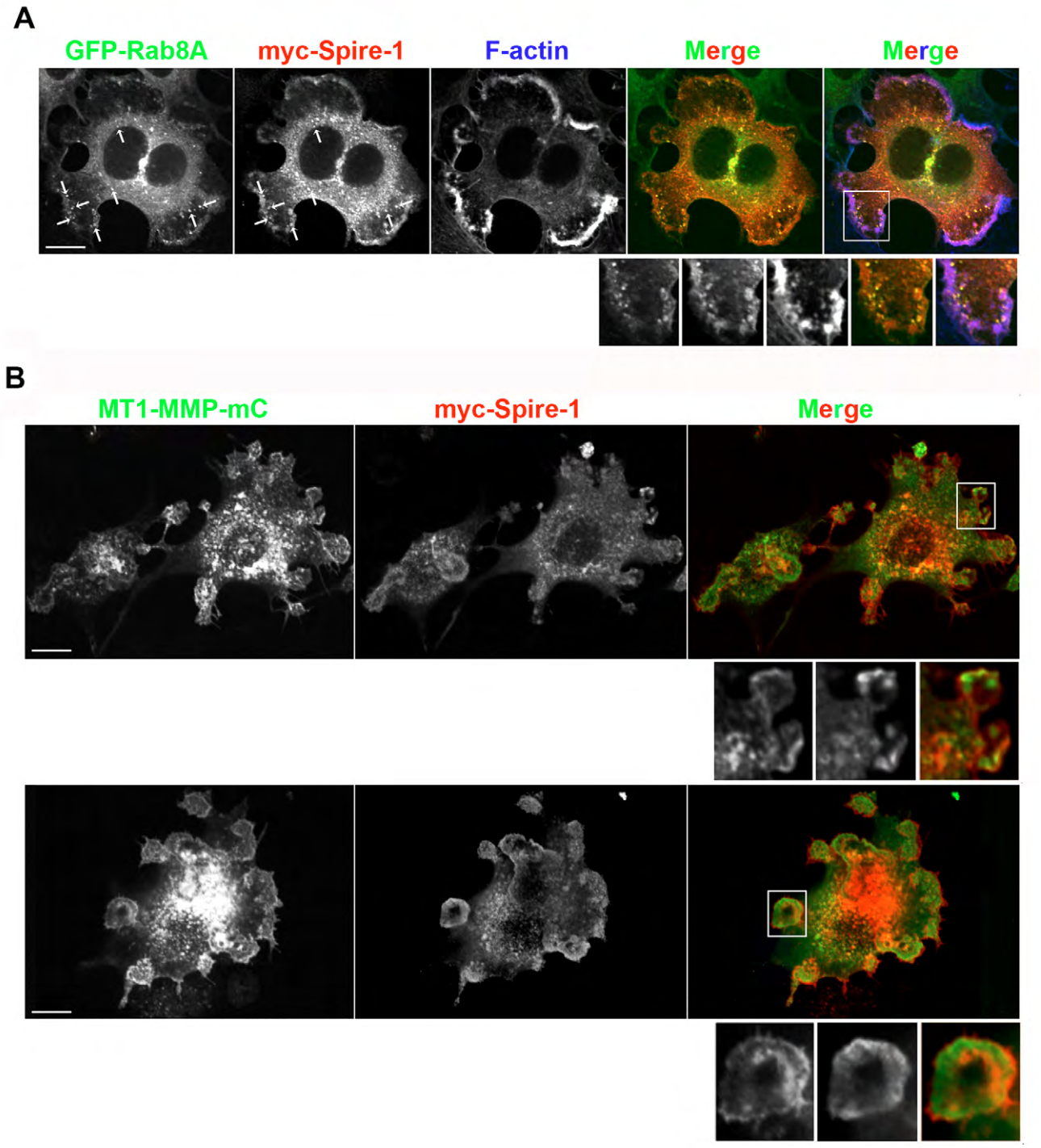


**Fig. S5. Myc Spire-1 partially overlaps with both GFP-Rab8A and MT1-MMP-mC cytoplasmic vesicles while they distribute separately at invadosomes in Src+ fibroblasts after transient transfection. (A) Triple immunofluorescent labeling of Rab8A (GFP tagged, green), myc-Spire-1 (anti-myc antibodies, red) and F-actin (Phalloidin, blue) Arrows show individual cytoplasmic GFP-tab8A and myc-Spire-1-positive vesicles. Framed area shown in the merge image is zoomed in the bottom panel focusing on invadosomes and a rosette. (B) Double fluorescent labeling of MTP1-MMP-mC (red) and myc-Spire-1 (anti-myc antibodies, red); note the delivery of the protease at the membrane surrounding the myc-Spire-1-positive invadosomes and rosettes. Frame area in the merge images are magnified in insets at the bottom of the panel. Scale bar: 10 µm**

**Table S1. List of primers used for PCR and cloning procedures**

| tGene | | PCR Primer sequences | |
|---|---|---|---|
| *ARP3* | | Forward-GAGAGACCGAGAAGTAGGAATCCC<br>Reverse-CTCAGGCGTGGAAGCCAGC | |
| *Spir-1* | | Forward- CTATGGTGAATGGAGGTTTGACATC<br>Reverse – GGCCTGGCGAGGACATGTAGAAAG) | |
| | | | |
| **Recipient vector** | **Insert (amino acid position)** | **PCR Primer sequences** | **Cloning sites** |
| pCDNA3-myc | Full length 1-756AA | Forward- GC GGA TCC ATG GCT CAG GCG GCT GGC CCG<br>Reverse- CG CTC GAG GAT CTC ACT GAT CGT CCT CTC T | BamH1/Xho1 |
| pEGFP-C3 | Full length 1-756AA | Forward-CCGCTCGAGATGGCTCAGGCGGCTGGCCCG<br>Reverse-GCTCTAGATCAGATCTCACTGATCGTCCTCTCT | Xho1/Xba1 |
| pCS2-MT-myc | WH2 268-480AA | Forward-CCGCTCGAGGACTGGGCACGATTCTGGGTAC<br>Reverse-GCTCTAGATCAGCTGCTGCTGCTGGTCGAC | Xho1/Xba1 |
| pCS2-MT-myc | C-terminal 556-756AA | Forward-CCGCTCGAGCTCGCTCTTACTGTGGAAGAAGTG<br>Reverse-GCTCTAGATCAGATCTCACTGATCGTCCTCTCT | Xho1/Xba1 |
| pCS2-MT-myc | WH2-Cterminal 268-756AA | Forward- CCGCTCGAGGACTGGGCACGATTCTGGGTAC<br>Reverse-GCTCTAGATCAGATCTCACTGATCGTCCTCTCT | Xho1/Xba1 |
| pCS2-HA | C-terminal 556-756AA | Forward-CCGGAATTCCTCGCTCTTACTGTGGAAGAAGTG<br>Reverse-GCTCTAGATCAGATCTCACTGATCGTCCTCTCT | EcoR1/Xba1 |
| pCS2-MT-myc | N-KIND 1-230AA | Sub-cloning from pGEX6p3-KIND | BamH1/Xho1 |
| pCS2-MT-myc | N-KIND-WH2 1-460AA | Sub-cloning from pGEX6p3-KINDWH2 | BamH1/Xho1 |
| pET2817-hGST | N-KIND 1-230 AA | Forward<br>CAGTCAGGAGCCATGGCTCAGGCGGCTGGCCCG<br>Reverse<br>AGTCAGTTAGGATCCGAGCTCCATTGTTTCTGCAAACAG | NcoI/BamH1 |
| pET2817-hGST | C-terminal 389-756AA | Forward<br>CAGTCAGGAGCCATGGTTAGACGTAGCAGATTAGCAATGC<br>Reverse<br>AGTCTGTTAGGATCCGATCTCACTGATCGTCCTCTCTGA | NcoI/BamH1 |

**SupTable 1: Lagal et al**.

**Table S2. List of antibodies used for in situ and biochemical analysis**

| Antibody | Dilution in Western Blot | Dilution for IFA | Source |
|---|---|---|---|
| Rabbit anti-Spire-1 | 1/1000 | | K-19, Santa Cruz Biotechnology **Inc.**Heidelberg, Germany |
| Rabbit anti-Rab3A | 1/2000 | 1/100 | Synaptic Systems, Goettingen, Germany |
| Mouse anti-GAPDH | 1/20000 | | Clone 6-C5, Ambion® Life Technologies, Saint Aubin, France |
| Rabbit anti-N-KIND-Spire-1 | 1/1000 | 1/100 | Amino acid 1-230, Eurogentec, Angers, France |
| Mouse anti-c-myc | 1/3000 | 1/200 | Clone-9E10, Santa Cruz Biotechnology **Inc.**Heidelberg, Germany |
| Rat anti-HA | 1/4000 | 1/600 | Clone-3F10, Roche |
| Mouse anti-cortactin | 1/5000 | 1/100 | Clone-4F11, Cell Signaling |
| Rabbit anti-Src phosphorylated (pY418) | | 1/200 | Cell Signaling |
| Mouse anti-Dia1 | 1/1000 | | Clone 51, BD Transduction laboratories, Pont de Claix, France |
| Mouse anti-p16 (ARP2/3 subunit) | 1/1000 | | Clone-323H3, Synaptic Systems, Gottingen, Germany |
| Mouse anti-Src | 1/1000 | | Clone GD11, Millipore, Molsheim, France |
| Mouse anti-actin | 1/2000 | | Clone-C4, Sigma-Aldrich, S$^{t}$ Quentin Fallaviers, France |
| Mouse anti-GFP | | | Roche Diagnostic, Meylan, France |
| Rabbit anti-GST | 1/20000 | | Sigma-Aldrich, St Quentin Fallaviers, France |
| Rabbit anti-Histidine | 1/5000 | | Santa Cruz Biotechnology **Inc.**Heidelberg, Germany |
| Mouse Ve-Cadherin | | 1/200 | clone BV6 \| MABT134, Millipore, Molsheim, France |
| HRP conjugated goat anti-rabbit | 1/10000-1/20000 | | Pierce Fisher Scientific, Illkirch, France |
| HRP conjugated goat anti - mouse | 1/20000 | | Pierce Fisher Scientific, Illkirch, France |
| Alexa Fluor-conjugated secondary antibodies | | 1/1000 | Invitrogen life Technology, saint Aubin, France |

**SupTable 2: Lagal et al.**

**Table S3. List and composition of buffers**

| Buffer Name | Composition | Use |
|---|---|---|
| **A** | 20 mM HEPES, 150 mM NaCl, 0.1% TX-100, 2 mM $MgCl_2$, 1 mM EDTA, 10% glycerol, 2X protease inhibitors | 4°C, 20 min |
| **B** | 50 mM Tris-HCl, 150 mM NaCl, 1 mM DTT, 2X protease inhibitors, pH-8 | 4°C, 30 min |
| **C** | 20 mM HEPES, 150 mM NaCl, 1 mM DTT, 10% glycerol, 1 mM EDTA, 1 mM $MgCl_2$, pH-7.4 | 4°C, 20 min |
| **D** | 20 mM HEPES, 150 mM NaCl, 2 mM EDTA, 0.2 mg/ml BSA, 10 mM $MgCl_2$, 1 mM DTT and 2X protease inhibitors, pH-7.4 | |
| **E** | 50 mM HEPES, 150 mM NaCl, 10 mM $MgCl_2$, 0.2 mg/ml BSA, 2X protease inhibitors, pH-7.5 | 4°C, 20 min |

**SupTable 3: Lagal et al.**